THE PHYSICS OF TSUNAMIS

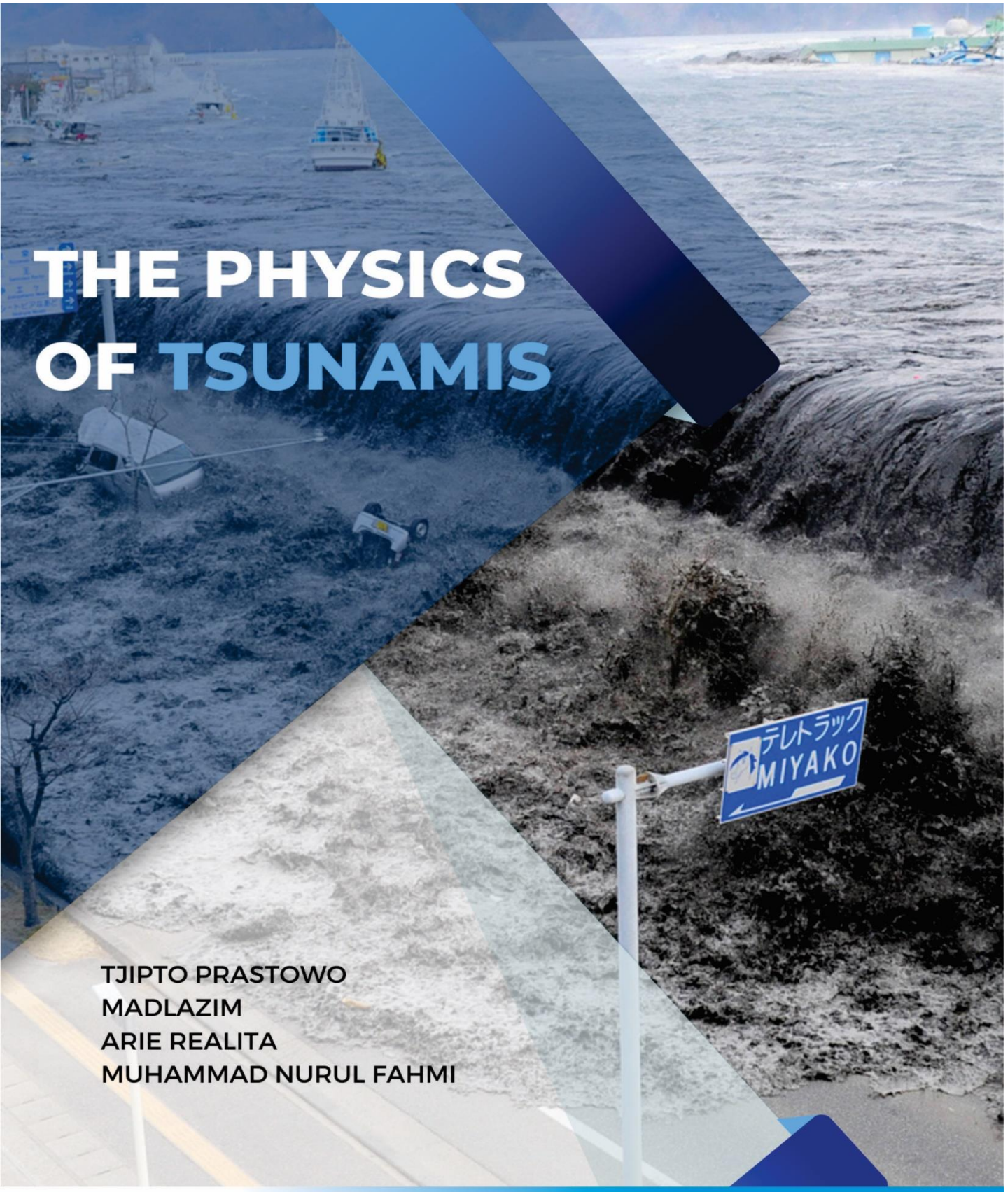

TJIPTO PRASTOWO
MADLAZIM
ARIE REALITA
MUHAMMAD NURUL FAHMI

THE PHYSICS OF TSUNAMIS

Tjipto Prastowo
Madlazim
Arie Realita
Muhammad Nurul Fahmi

Penerbit:
Pondok Pesantren Jagad 'Alimussirry (Anggota IKAPI)
"Komunitas Ilmuan Spiritualis"

THE PHYSICS OF TSUNAMIS

Penulis:

Tjipto Prastowo
Madlazim
Arie Realita
Muhammad Nurul Fahmi

ISBN : 978-602-

Desain Cover dan Layout:

Aris Handriyan, S.Si, M.Pd

Penerbit:

Pondok Pesantren Jagad 'Alimussirry (Anggota IKAPI)

JI. Jetis Kulon VI/ 16 A Surabaya 60243

Telp. 031.286562

e-mail: penerbitjagadalimussirry@gmail.com

Cet. 1 (Pertama): 12 Oktober 2023

DAFTAR PUSTAKA

Segala puji dan syukur kami panjatkan kehadirat Allah SWT yang telah melimpahkan segala anugerah dan rahmatNya sehingga tim penulis dapat menyelesaikan buku dengan judul **The Physics of Tsunamis.**

Buku ini akan mengulas tentang seluk beluk Tsunami meliputi: proses terbentuknya tsunami, wilayah-wilayah yang memungkin terdampak oleh adanya tsunami, kecepatan tsunami, ciri-ciri gempa yang dapat menyebabkan tsunami, bentuk-bentuk mitigasi dari adanya bencana tsunami. Setelah membaca buku ini diharapkan memberikan manfaat bagi pembaca, khususnya bagi orang-orang yang tinggal di daerah pesisir pantai untuk bisa siaga dan mempersiapkan diri untuk menghadapi jika datang tsunami.

Penulis menyadari bahwa buku ini masih banyak memiliki kekurangan baik substansi maupun organisasi tulisan. Oleh karena itu, kritik yang membangun sangat diharapkan untuk kesempurnaan buku ini kelak. Semoga buku ini dapat bermanfaat tidak hanya bagi penulis melainkan juga bagi para pembaca yang berminat.

Surabaya, Oktober 2023
Tim Penulis

CONTENTS

Chapter One

DYNAMIC ZONES OF TSUNAMIS

The strong ground motion following the M_w 9.1 underwater earthquake of the boxing day on 26 December 2004, located off the west coast of Nanggroe Aceh Darussalam (NAD) in the northern Sumatra Island, and the resulting destructive tsunami wave produced one of the major earth-related disasters in the world. In the context of global community, the causative earthquake is well-known as the 2004 Sumatera-Andaman event whereas the corresponding tsunami is commonly called the 2004 Indian Ocean tsunami. In terms of fatalities, this event is considered to be the most devastating tsunami with a total of around 230,000 deaths accounted in affected regions, mostly in South and Southeast Asian countries, including Indonesia and its nearby coastal countries.

Owing to its geological conditions induced by seismotectonic settings, the vulnerability of Indonesian territory to tsunamis is well described by the 2004 Indian Ocean tsunami. Therefore, it is important to study tsunamis in greater details, examining the waves from the beginning with the basic level of understanding to a higher level of views throughout the book. This chapter, however, focuses on three regimes of dynamic zones of tsunamis, namely (1) zone of generation; (2) zone of propagation; and (3) zone of mitigation.

1.1 Zone of Generation

A zone of tsunami excitation is a place in the open ocean, where a tsunami is generated. The principal mechanism of tsunami generation is the large displacement of ocean water masses or volumes in the entire water column. This mechanism is basically different from wind-generated waves, where only surface layers of the ocean are directly perturbed by the wind. In the case of tsunami generation, such initial displacement of the water involves a huge amount of energy supply, for which the displacement is attributable to submarine earthquakes, subaerial or submarine landslides, and volcanic eruptions to mention the most common causes, which will be discussed in details in Chapter Two. The wave formed is sustained by gravity in the following steps. When a water column is disturbed in the vertical direction, the gravity acts to return the surface to the equilibrium and in turn the returning surface oscillates. This oscillation disturbs the adjacent surface, finally causing the horizontal wave propagation. In all occurrences, ocean tides do not play a role in tsunami generation.

Here is a more description of tsunami generation. When seafloor deformation abruptly occurs following an underwater tectonic earthquake, the overlying water column is then vertically displaced from its equilibrium. This displaced water column disturbs stably stratified layers of ocean waters from the ocean bottom to the surface and the next step is precisely about to occur as it is previously written. Hence, it is obvious that the size of the vertical displacement of ocean water masses or volumes (induced by the energy released from thrust faults associated with convergent plate boundaries near or along the subduction zone) takes part in giving rise to a resulting tsunami wave.

However, when examining tsunamis generated by undersea earthquakes, of particular interest for some reason is a relationship between a causative earthquake magnitude and its resulting maximum tsunami amplitude. It is possible to parameterise the magnitude measured in moment magnitude M_w with the spatially averaged tsunami amplitude η recorded by instrumental surface buoys and tide gauges, distributed over large areas in an ocean-wide basin for tsunami monitoring. Recent studies (Heidarzadeh et al., 2018; Prastowo et al., 2022) have investigated this issue using trans-oceanic tsunamis and found that $M_w \sim \log \eta$ with a slight difference in the details of the parametric equations for tsunami cases across the Pacific and the Indian Oceans. The apparent difference is thus attributable to differences in both topographic complexity and tsunami directivity in the two oceans.

1.2 Zone of Propagation

A zone of tsunami propagation is a region in the ocean, where a tsunami is propagating. Once generated, a tsunami wave can propagate in all directions from the source area, carrying a huge amount of energy with it. While wind-generated waves have a relatively short wavelength of about 100 m and a height of up to 4 m measured from the sea level, a tsunami wave in the ocean has a very long wavelength in the order of about 200 km with the period may take 15 to 20 minutes (relatively compared to a couple of minutes for wind waves) to complete the oscillation. Tsunamis have a relatively small amplitude (sometimes in the literature referred to as tsunami wave height) in the open ocean (or in general offshore) that may be observed under a meter high from the surface, making it barely noticeable even if a travelling ship sails across the ocean during tsunami passage. However, the amplitude grows in height whenever it reaches waters of shallower depth. This is to occur due to depth dependence of tsunami speed. When approaching onshore with shallow waters, tsunamis slow down but interaction with the topography increases dramatically the wave height to keep volume conservation running (see Figure 1.1).

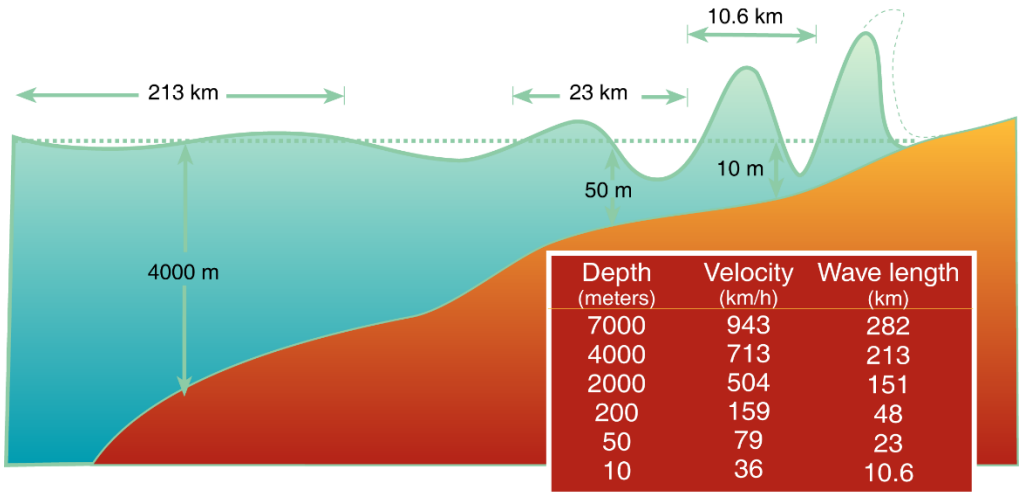

Figure 1.1. Sketch showing a propagating tsunami wave (from left to right sideviews) approaching the shoreline with relatively shallow water. The topography compresses tsunami wavelength, reducing the speed but amplifying the amplitude for volume conservation (source: http://itic.ioc-unesco.org/index.php?option=com_content&view=category&id=1340&Itemid=1138#:~:text=By%20far%2C%20the%20most%20destructive,subduction%20along%20tectonic%20plate%20boundaries).

In the context of the depth-dependent speed (where the speed is equal to the square root of gravitational acceleration multiplied by water depth), in the deep ocean with a typical depth of 4000-5000 m, a tsunami propagates at speeds of approximately 200-220 ms^{-1} or 720-800 ms^{-1}, even in some circumstances it is capable of travelling at a higher speed (see Santellanes et al., 2022; Hu et al., 2023). While tidal waves have no effects upon tsunami excitation, tsunami propagation is possible to be influenced by tides, as well as storm surge conditions but the details of influences are not here provided. That is why tsunami wave height records obtained from field observations must be reported with additional information whether tsunami passage is coincidence with high tides.

Although global tsunami events are commonly generated by subduction earthquakes in the open ocean (followed by tsunami propagation), tsunamis may be induced by other sources in relatively wide straits, such as the case of the 2018 Sunda Strait tsunami (Muhari et al., 2019) and even in the vicinity of the inlet of a relatively narrow bay, such as the case of the 2018 Palu Bay tsunami (Gusman et al., 2019) to mention two examples that occurred in Indonesia. In these cases, the speed varies with water depth during tsunami propagation. We leave detailed discussions of possible approaches used for speed determination till Chapter Three, after which we examine effects of varying speeds on tsunami travel time hence arrival time, discussed in details in Chapter Four.

1.3 Zone of Mitigation

A zone of tsunami mitigation is a region in the coastline, where a tsunami is arriving at the coasts and in turn will inundate large parts of inland. As the rate at which wave energy is dissipated is inversely proportional to wavelength, tsunamis can travel great distances with only a limited loss of the energy. Like wind-generated waves, tsunami energy is also transported during propagation and transferred into reflected waves when hitting ocean obstacles, such as islands and shores, and only a small part of the energy is converted to heat due to bottom friction between the wave and seafloor. With small energy reduction, tsunamis remain coming to shorelines with enormous energy, possibly eroding beaches, undercutting coastal vegetation and inundating low-lying land at far distances, leading to potentially economic losses of properties and human lives.

When the wave approaches coastlines with shallow water depth, a wave shoaling process compresses the wave, shortening the wavelength and reducing the speed significantly. The approaching wave does not break but rather appears to be a fast-moving tidal bore. As a result, when arriving onshore the wave amplitude increases enormously to preserve the flux of energy and is usually called run-up, as seen in Figure 1.2. A tsunami in nature may feature a series of travelling waves with varying wavelengths and a significant time between the wave arrivals. The first arrival to reach a particular shore may not come with the maximum amplitude hence the highest run-up. We leave detailed discussions of possible approaches used for run-up estimates in Chapter Five. For now, it is adequate to say that the wave height at the shoreline is called tsunami run-up and the horizontal distance the wave travels inland is termed tsunami inundation.

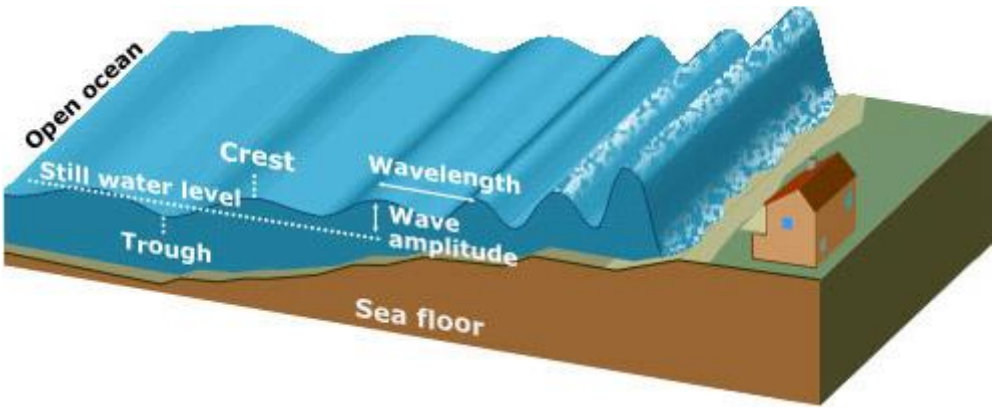

Figure 1.2. Sketch showing a tsunami wave approaching the shoreline with all consequences of shoaling effects, including speed reduction and increased wave height called run-up (taken from http://tsunami.org/tsunami-characteristics/).

When the first part of the wave to reach on land in the coastal areas is a trough rather than a crest, then the surface water along the shorelines recedes dramatically, a common phenomenon called a drawback. A drawback begins before the wave arrives at a time which is equal to the half of the wave period and can exceed hundreds of metres, where people are unaware of serious danger to come. In fact, a drawback can serve as a warning. One who observes a drawback can survive only if they immediately run for high places. A boy/girl of ten-years old from England was on playing around the beach in Phuket, Thailand with his/her parents. The boy/girl had learned about tsunamis in school and he/she told her family that a giant wave might be imminent. His/Her parents warned others minutes before the first wave arrived, preventing dozens of lives from vain deaths.

The above story is a good example of how science literacy is effectively improved with geoscience education at any level from primary to tertiary education. Such education is a cornerstone for introducing the way in which we manage tsunami-induced problems and mitigation strategy, particularly when we are living in or staying close to a vulnerable coastal region to tsunamis. In addition, vital roles of relevant agencies and regulations as well as roles of universities and academics are all discussed in details in Chapter Six, the end of the book.

1.4 Concluding Remarks

Research on topics associated with tsunamis has been recently accelerated in response to a devastating tsunami that occurred on the boxing day of 26 December 2004 in NAD. In the last twenty years, more destructive tsunamis occurred worldwide that argued for the best assumptions for a better understanding of tsunami generation, propagation, and inundation. The close link between shallow subduction zones and tsunami generation naturally lead to a focus on this type of source for the first-time examination. However, current tsunami research has included: (1) source mechanisms other than subduction earthquakes, including inland shallow crustal strike-slips and thrust-fault earthquakes; (2) subaerial and submarine landslides; (3) volcanic eruptions and even factors affecting tsunamis from meteorological events; (4) site effects (such as local coastal topography and shelf geometry) on tsunami propagation and inundation. The expansion of tsunami research has shown that tsunami generation and propagation are more complex than previously thought. For comprehensive tsunami hazard analysis and its associated risks, it is important that all tsunami generation and propagation mechanisms are understood, as well as corresponding strategy for tsunami mitigation. All of these source mechanisms

that influence tsunami generation and propagation (both offshore and onshore) will be discussed in details in the next chapters.

1.5 Exercises

Answer clearly to the following questions regarding the content of Chapter One.

1. Imagine someone is about to say zones of tsunami generation, tsunami propagation and tsunami mitigation. Then what do you want to say about the three dynamic zones of tsunamis to complete information.
2. Why are most tsunamis generated in regions near or along the convergent plate boundaries ? Is it possible to find a place other than the convergent plate boundaries, where a tsunami may be generated ?
3. For non-dispersive tsunami waves with the wave speed depends only on water depth, why does the speed reduction lead to an increase in the wave height when the waves arrive onshore ?
4. What is the best thing to do you may think of regarding tsunami warning ?

Chapter Two

POSSIBLE SOURCES OF TSUNAMI EXCITATION

This chapter describes tsunami waves, which can be generated by some possible sources: either tectonic earthquakes, subaerial and submarine landslides, or volcanic eruptions. Direct impacts on the nearby coastlines and human population are clearly devastating, resulting in substantial losses of many properties and lives induced by tsunamis of any source mechanism. Tsunamis and their potential impacts have received considerable attention in the world after a catastrophic tsunami occurred in NAD Province, Indonesia on 26 December 2004, then followed by two major earthquake-tsunami occurrences in Maule, Chile on 27 February 2010 and in Tohoku, Japan on 11 March 2011. Regarding the rarity of a major tsunami event, it is remarkable to note that the 2010 Maule, Chili and the 2011 Tohoku, Japan tsunamis occurred within only one year time spanning. Except for the 2004 Indian Ocean tsunami, the Pacific Ocean is the most vulnerable to future large tsunamis due to the frequency and magnitude of tectonic earthquakes that possibly occur near and along the pathway of the Pacific Ring of Fire. Minor tsunamis are also found to occur worldwide but they are rarely discussed by tsunami community since no significant losses and fatalities in effects are reported.

2.1 Source 1: Earthquake of Tectonic Origin

Tsunamis are usually generated by large earthquakes of shallow source with an epicentre or a faulting line near or on the ocean floor, for which the earthquake source mechanism is referred to underwater fault movement that causes vertical ocean bottom deformation (see Figure 2.1). These events are frequently observed to occur in regions characterised by a subduction zone along major tectonic plate boundaries, where the underlying plate subducts beneath the other plate. Most destructive tsunamis in the world originate from the Pacific Ring of Fire, a pathway of convergent zones along the perimeter of the Pacific. Once a tsunami is generated, the propagating wave can travel over great distances from the source area with limited losses of energy and high speeds of more than 800 km/h, spreading destruction along its path. For instance, the 1960 Valdivia earthquake with magnitude of M_w 9.5 caused a destructive tsunami, hitting not only the west coastlines of Chili but also as far away as the coasts of Hawaii, Japan and elsewhere in the Pacific.

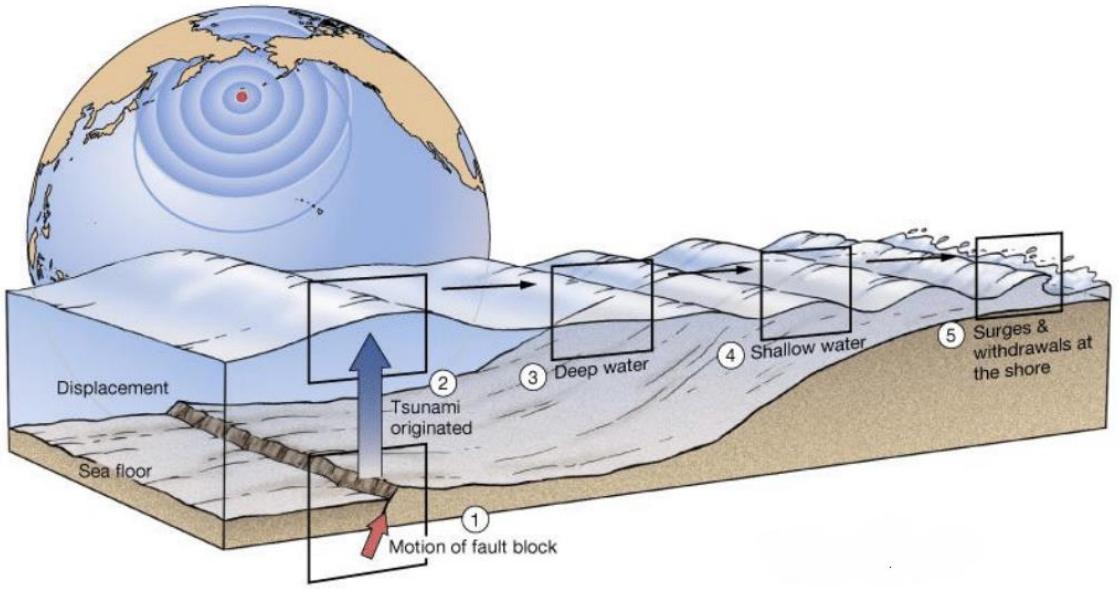

Figure 2.1. Sketch showing underwater fault movement during a sudden drop of a fault block relative to another hanging fault block that takes place near the sea floor. The energy released from the drop displaces large volumes of ocean water column from near the bottom to the surface, disturbing ocean water level and in turn generating a propagating tsunami wave (taken from Chapter 8 of Essential of Oceanography by Alan P. Trujillo, Harold V. Thurman, 2008).

Three cases considered are the 2004 Indian Ocean, Indonesia; the 2010 Maule, Chili and the 2011 Tohoku, Japan tsunamis. These tsunamis were generated by earthquake events. We begin discussion on the first case with aspects associated with tsunami generation, size and extent, and impacts. Tsunamis induced by seismotectonic activity are very rare in the Indian Ocean, relatively compared to the those in the Pacific Ocean.

Nonetheless, the 2004 Indian Ocean tsunami that occurred at about 8:30 am local time remains the deadliest tsunami ever recorded in the history. This tsunami was triggered by the 2004 Sumatera-Andaman earthquake of M_w 9.1, having the epicentre at 250 km off the north-west coast of Sumatera Island along the subduction zone of the marginal Indo-Australian and Eurasian plates and the depth at about 30 km below the surface. The earthquake source ruptured for a time duration of ~8 min with a total rupture extent of about 1,300 km, triggering a tsunami wave that reached up to 30 m in height and caused at least 230,000 fatalities in many African and Asian coastal countries, such as Indonesia, Sri Lanka, Thailand, Maldives. One of lessons learned from this deadly event is developed after thorough post-event examination. Sensitive monitoring instrument for both near-field and far-field tsunami hazard analysis and corresponding assessment

for a quick, emergency response to tsunami early warning is required. The importance of such sensitive instrument deployment in the Pacific and Indian Oceans is thus a must with no exception. Tsunami excitation from other possible sources is also examined after the devastating 2004 event although the early warning system in its initial development was practically designed for tectonic earthquake-tsunamis.

The second case discussed is a tsunami that was triggered by the earthquake of M_w 8.8 having the epicentre 3 km off the coast of Maule, central Chile on 27 February 2010 at 03:34 am local time at a depth of about 35 km, with strong ground shaking lasting for about 3 minutes (much shorter duration compared to the 2004 Indian Ocean tsunami). This earthquake was characterised by a thrust-faulting mechanism, driven by the active Nazca Plate subducting beneath the South American Plate. The fault segment, which ruptured in this event was estimated to be 700 km long (about half of rupture extent of the 2004 Indian Ocean tsunami). Field measurements demonstrated that the whole South American Plate shifted abruptly westward following the earthquake. The resulting 2010 Maule tsunami amplitudes were observed to range from a few to several tens of centimeters while field surveys reported run-ups of up to 15 m along the Chilean coasts. The tsunami wave reached the Japanese coastlines after travelling across the Pacific in about 23 h with the observed tsunami heights of up to 2 m. Reported fatalities included 525 people lost their lives while many others got seriously injured.

The last case to consider is the 2011 Tohoku-oki, Japan tsunami. This tsunami event was triggered by the so-called Great East Japan subduction earthquake of M_w 9.0 (the largest in the Japanese history) that occurred on 11 March 2011 at 14:46 local time with a depth of 32 km below the ocean floor off the east-coast of Honshu Island, Japan. The source mechanism of the earthquake is thrust-faulting at the interplate boundary. The epicentre was located 72 km east of Oshika Peninsula in Tohoku in the northeast part of Honshu. Historically, this region is in fact considered seismically active with previous substantial earthquakes and tsunamis several times hitting the region. The earthquake was powerful enough to shift parts of Honshu Island 2.5 m eastward. Faulting area of 500 km long (north to south) and 200 km wide (east to west) at the plate boundary was ruptured for about 6 minutes. This caused significant vertical displacement of massive ocean water masses, leading to a tsunami that killed more than 20,000 people, leaving thousands were severely injured in Japan. Post-even field surveys indicated that tsunami run-ups were observed to reach a maximum height of approximately 40 m. The tsunami spread over the entire Pacific Ocean as it was reported to arrive at the Chilean coasts.

2.2 Source 2: Subaerial or Submarine Landslide

In general, the propensity for landslides of any type and source mechanism to occur is largely affected by potential slip planes, or weakness planes in the geological substrates, where the driving forces exceed the resisting forces. A landslide across the landscape is frequently unpredictable. Substrates can be resistant to slippage for a long time and then suddenly experience slope instability resulting from both human or non-human cause that disrupt the force balance between driving and resisting forces acting on a slip plane. In the geological context, landslides of any type are normally to occur on sloped terrain, making the local topography important for a landslide event. The underlying factors, however, that control whether or not a landslide occurs, include the local soil conditions and rock substrates. Detailed discussions on this issue are not provided in this section, rather we discuss the possibility of tsunami generation following causative landslides.

Massive landslides occurring near the ocean waters are able to generate large tsunamis and potentially endanger local human lives and properties, as empirically evidenced by historical landslide-tsunami events worldwide. Depending upon the relative position of the landslide with respect to the water surface, landslide-tsunamis can be classified into subaerial, submerged, and partially submerged tsunamis. Subaerial landslide-tsunamis are referred to landslide-tsunamis where all the causative body masses that slid down into the water are initially positioned above the water surface while the other two types of landslide-tsunamis are classified into submarine landslide-tsunamis (see Figure 2.2). In some literature and published papers, however, submarine landslide-tsunamis are associated with submerged landslide-tsunamis.

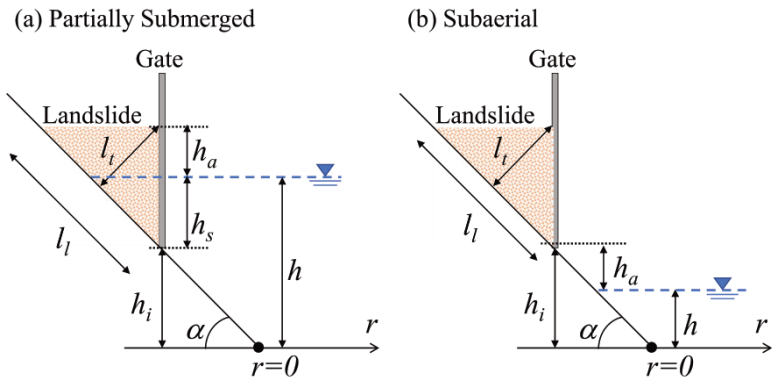

Figure 2.2. Diagram showing experimental set-up for (a) partially submerged and (b) subaerial landslide-tsunamis (taken from Takabatake et al., 2022). Notice that inverted triangles indicate the water surface and other symbolised parameters written are not important for differentiating the two source mechanisms.

An example of a subaerial landslide-tsunami occurred in Chehalis Lake, Canada in 2007. The 2018 Palu Bay case was a good example of a submerged landslide-tsunami following an M_w 7.5 strike-slip earthquake having the epicentre located about 80 km to the north of Palu City on 28 September 2018 (see Figure 2.3). The so-called 2018 Palu Bay tsunami has been in debate in terms of the exact source mechanism whether the tsunami was triggered by the earthquake, the submerged landslide, or a combined mechanism of both. The left-lateral strike-slip faulting source mechanism with approximately north-south orientation obtained from the global Centroid Moment Tensor solution is consistent with the relative motion of active Palu-Koro Fault.

Relative to the mainshock, the aftershocks are mostly positioned to the southeast, hence showing a northwest-southeast trendline with a total length of approximately 200 km. Although strike-slip faulting earthquakes are usually reported to induce small tsunamis owing to the relatively small energy supply for the vertical ocean bottom deformation, the Palu-Donggala earthquake generated large tsunamis along the coastline of Palu Bay, known as a narrow bay with a total length of ~30 km and a maximum width of ~7 km. Regarding the location of the epicentre, about 55 km to the north of the inlet of Palu Bay, the front of high-frequency seismic radiations bringing energetic seismic waves arrives at the inlet before entering the bay. This is consistent with the predicted locations of submarine landslides, which is just outside and within the bay to form the dual sources of localised tsunamis. This argument, along with multiple wave reflection within the bay owing to its geometry (Fahmi et al., 2022), could be the answer to the question of why such an event generated unexpectedly high tsunami waves, where the western shorelines of the bay are mostly influenced by the tsunami. The National Disaster Management Authority (BNPB) has reported that 4,340 people were killed and 10,679 were injured by either or combinations of the tsunami, landslide, liquefaction, and collapsing building following the earthquake, and 667 people have been declared missing.

Post-tsunami field surveys following the 2018 Palu-Donggala earthquake and tsunami were then performed by international groups to measure tsunami heights, impacts, and collect eyewitness accounts. The tsunami waves were also detected by a tide gauge station at Pantoloan harbor located inside Palu Bay (see Figure 2.3). Satellite images before and after the event, freely accessed at https://www.digitalglobe.com/ecosystem/open-data, provide a better look to identify the damage extent and the limit of horizontal inundation. The Geospatial Information Agency of Indonesia (BIG) has found locations of destroyed and damaged buildings around Palu from a rapid assessment using the satellite imagery.

The video footage provides additional information about the deadly event. All necessary documents were well-documented for lesson learned from the Palu Bay tsunami event.

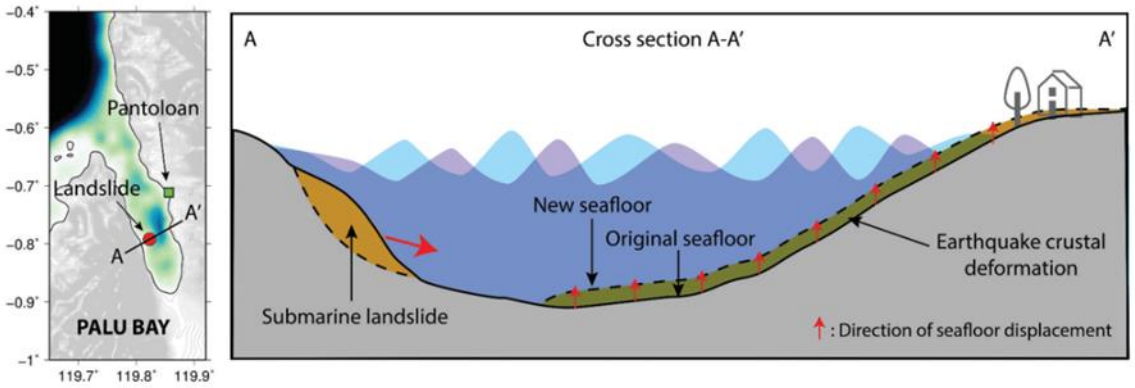

Figure 2.3. Sketch showing the combined earthquake and submarine landslide model proposed for the 2018 Palu Bay tsunami (taken from Heidarzadeh and Mulia, 2022).

A partially submerged landslide of Anak Rakata in Sunda Strait (see Figure 2.4) had been numerically predicted to induce tsunami hazards 6 years before it was reported to excite a volcanic tsunami due to a flank failure, following slope instability of the active volcano on 22 December 2018. On the day it occurred, Anak Rakata volcano experienced a major lateral collapse during a period of eruptive activity that began in June. The flank collapse discharged volcaniclastic materials into the 250 m deep caldera southwest of the volcano, which generated a tsunami with run-up of up to 13 m on the west coastlines of Java and the south coastlines of Sumatra. The resulting tsunami wave caused at least 437 fatalities, compared to 36,000 deaths reported during the 1883 Krakatoa case. For the first time in over a century, the 2018 Sunda Strait event provides insight into a major volcanogenic tsunami that caused regional significant building damage in affected areas, in addition to losses of lives and properties.

Although the relationship of the landslide source mechanism and tsunami propagation in the case of the 2018 Sunda Strait tsunami remains poorly known hence is challenging to examine, some influentially linked factors that may have predisposed the volcano for the flank collapse of its southwest slope are here discussed. First, its existing position on the northeast margin of the caldera, formed from the 1883 Krakatoa explosive eruption, has resulted in steeper submarine slopes to the southwest compared to the northeast. Second, there has been a gradual shift in the vent position during its evolution towards the southwest and the interior of the caldera. Third, significant portions of lava flow deltas have extended Anak Rakata base to the west, which overlie potentially weak and

altered volcaniclastic materials produced by the 1927-1960 Surtseyan eruptions. Finally, the rapid growth of the volcano during the last 90 years have built a steep-sided summit on the west flank, consisting of dominant, unstable volcaniclastic materials. Therefore, it is safe to say that slope instability exists in the south-west side of the volcano flank. The partially submerged landslide-tsunami modelling on the basis of the flank failure in the south-west is consistent with a tsunami source of 0.22-0.30 km^3 (Grilli et al., 2019), sliding down into the 1883 caldera estimated from the post-collapse imagery (note that an estimate of 0.28 km^3 volcaniclastic materials for comparison was previously proposed for the 2012 predicted volcanogenic tsunami by Giachetti et al., 2012).

In short, among the three landslide-induced tsunamis, the subaerial type has been most studied using laboratory and computational work as it is relatively easy to set up the run. The generation process of a submarine landslide-tsunami is basically different from that of a subaerial landslide-tsunami. However, wave dispersion effects on the characteristics of tsunami propagation for all types of landslide-induced tsunamis are significant during the propagation, leading to propagation similarities in all the source mechanisms.

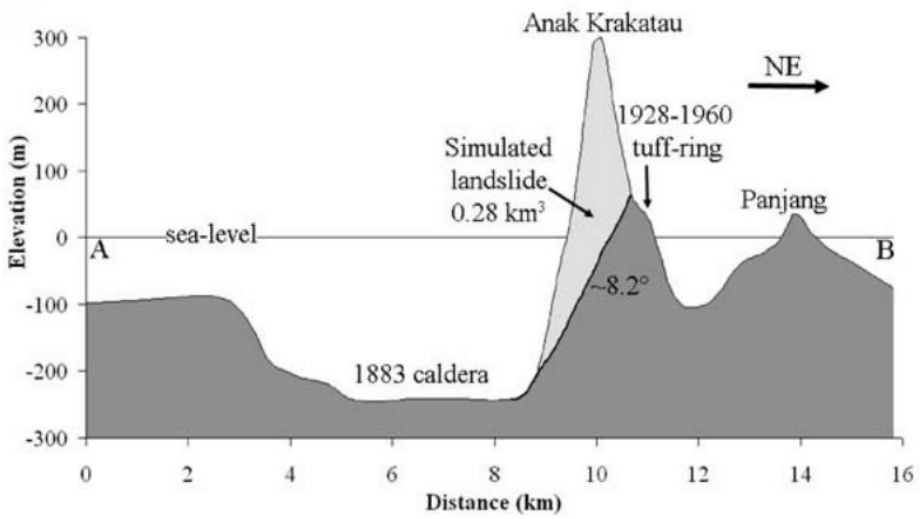

Figure 2.4. Sketch showing the partially submerged body of Anak Rakata volcano that collapsed on 22 December 2018 and generated a tsunami wave following a series of volcanic eruptions from months to days before (taken from Giachetti et al., 2012).

2.3 Source 3: Volcanic Eruption

As widely known, tsunami early warning system is designed mainly to detect tsunamis triggered by earthquake of seismic origin (see §2.1 for Source 1). This warning system is primarily based on automatic data processing of earthquake source location in a zone of

tsunami generation; tsunami amplitude, travel time and arrival time in a zone of tsunami propagation; and simulations of run-up and inundation in a zone of tsunami mitigation. Although the development of the system is in progress, it is not well-suited to deal with other generators, such as submarine or terrestrial landslides and volcanic eruptions. Considering all possible sources for an accurate, probabilistic tsunami hazard analysis is thus challenging as it requires different source mechanisms of tsunami generation and different monitoring techniques to run, including those related to volcanic tsunamis.

While tsunamis in general have 15-20 minutes for periodicity, tsunamis associated with volcanic processes are indicated by shorter-period waves. Volcanic tsunamis have also greater dispersion and limited effects on distant observations relatively compared to tectonic earthquake-generated tsunamis. Like other potential sources, volcanic tsunamis are also difficult to predict with the time available for issuing an alert is often very short, typically only a few minutes. Modern records reported that most volcanic eruptions near the coasts are not tsunamigenic but once it occurs, the cause of the tsunami is likely to be uncertain and the data from post-tsunami field surveys are difficult to interpret.

This section considers volcanic tsunamis to be the ones generated by a variety of source mechanisms related to eruptive processes, including: (1) volcano-tectonic earthquake; (2) slope instability; (3) pyroclastic flow; (4) underwater explosion; (5) atmospheric shock waves; and (6) caldera collapse, as illustrated in Figure 2.5. We examine lessons learned from past eruptive events and address the influence of some parameters on tsunami generation. The diversity of the waves in terms of their amplitude, period and dispersion derived from each mechanism poses difficulties in building reliable numerical models and probabilistic tsunami hazard maps (Paris, 2015). The following paragraphs detail all the source mechanisms of volcanic tsunamis.

Earthquakes occurring before and during volcanic eruptions are, according to records, held liable for only one fifth of volcanic tsunami cases in the world. However, examples of these events are not well documented while other possible mechanisms might be implied in tsunami generation, such as the 1914 tsunami in Sakurajima Bay, Japan and the 1916 tsunami at Stromboli, Italy. Owing to the lack of instrumental records and hence the collected data, these past earthquakes were classified into unwell-defined events, making them difficult to judge whether they were volcano-tectonic occurrences or purely tectonic ones. Among all types of earthquakes associated with volcanic processes, only volcano-tectonic earthquakes can produce surface deformation large enough to generate a tsunami. These earthquakes result from accumulated stresses following magma ascent

and are characterised by a series of shallow seismic swarms. In short, earthquakes of any origin may induce slope instabilities and therefore indirectly generate tsunamis.

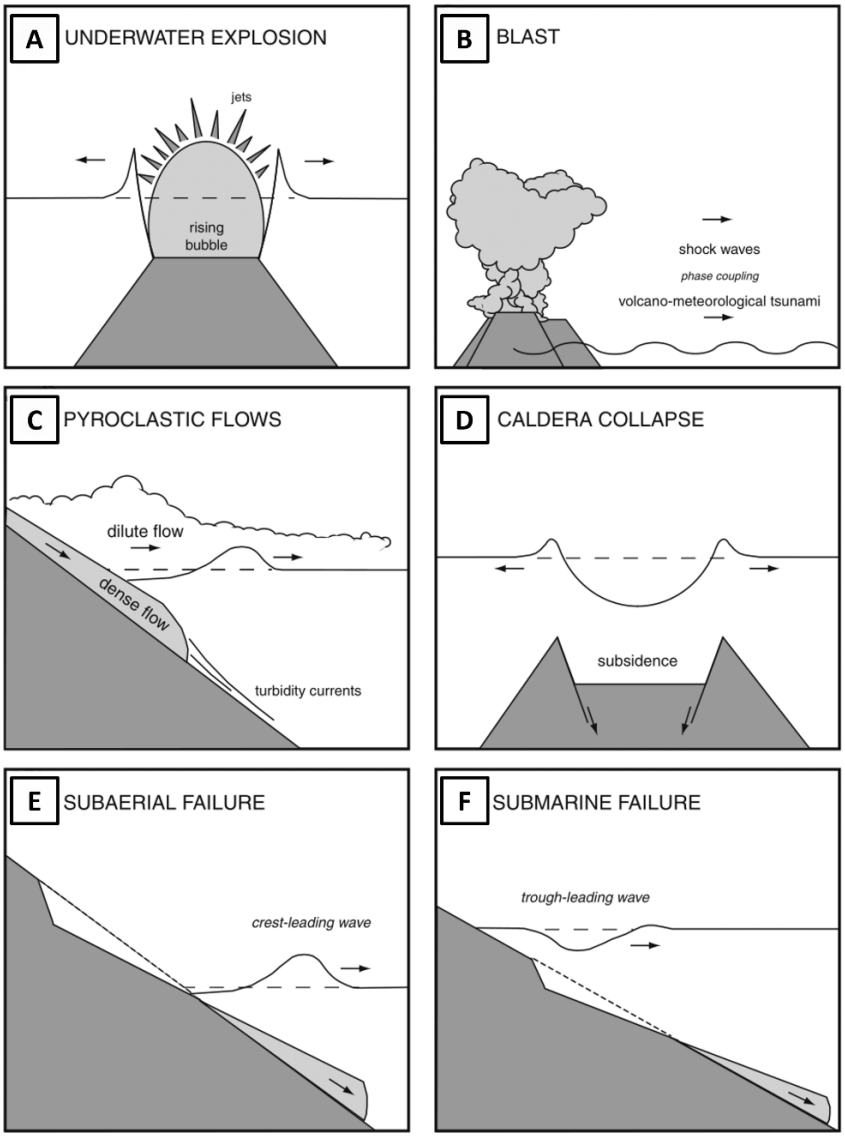

Figure 2.5. Diagram showing volcanic tsunami generation due to some possible sources (taken from Paris et al., 2014). Note that underwater explosion in (a) can be natural, such as a submerged volcano beneath the surface or human-induced, such as a nuclear bomb test; explosive eruption in (b) can produce shock waves creating atmospheric waves and in turn inducing tsunami waves called meteo-tsunamis; while a turbidity current from dense volcanic materials advances along the ocean bottom, a dilute flow propagates at the surface as a tsunami wave in (c); a tsunami may be generated when a caldera of a submerged volcano collapses in (d); the principle difference in the front between a crest-leading tsunami in sub-aerial mass failures in (e) and a trough-leading tsunami in submarine mass failures in (f).

A notable example of how slope instability of a submarine volcano is suspected to induce a tsunami was a tragic tsunami event on 22 December 2018 owing to a flank collapse of Anak Rakata in Sunda Strait following a series of eruptions from months to days before. Because the existing Indonesian tsunami early warning system was mainly designed for detecting earthquake-induced tsunamis, the system did not provide any alarm to warn people at risk. The precise source mechanism of the 2018 Sunda Strait tsunami remains unresolved as to whether it was generated by a single caldera collapse or retrogressive mass failures from the slope as the seismic station near the volcano was off, presumably due to damage following the eruption days before.

The post-tsunami field surveys and spectral analysis were then used for a comprehensive aftermath analysis (Muhari et al., 2019). The maximum distance of inundation was found to be 330 m and the maximum run-up was measured to be 13.5 m. Major damage in small islands close to the volcano indicates that the islands may have reduced tsunami amplitude and hence the energy before the waves arrived at the west coast of Banten and the south coast of Lampung. Waveform analysis revealed that the 2018 volcanic tsunami was a short-period wave, with the period ranging between 6.6–7.4 minutes, shorter than those from earthquake-generated tsunamis (as stated earlier in this section).

Tsunamis generated by volcano flank failures or slope instabilities are accounted for only 15% of total volcanic tsunamis recorded in the world. The usual mechanism is associated with the flow of mass failure from the slope into ocean water that subsequently generates a tsunami wave. This type of tsunami is arguably called ‘landslide-induced tsunami’ with its characteristics depend on the material origin (subaerial or submerged) and dynamics (initial acceleration, maximum velocity, deformation). Landslide-induced tsunamis of this type usually generate short-length and short-period waves with far-field propagation is limited by dispersion (as previously mentioned).

Pyroclastic flows are hot mixtures of volcanic gases and particles generated by eruptions following a volcanic dome collapse. These flows may enter the ocean water and propagate underwater as turbidity currents over intermediate distances. However, mechanisms of interaction between pyroclastic flows and water as well as the conditions required for tsunami excitation remain questionable as observations of this complex phenomenon are limited, in line with a lack of experimental and theoretical studies. The important parameters controlling the interaction of pyroclastic flows and water bodies are the bulk density of volcanic materials constituting the flow and its preservation or disaggregation underwater, the discharge rate, the angle of incidence and the distance from the vent.

Rapid discharge of pyroclastic flows into Sunda Strait waters from the 1883 Krakatau explosive eruption posed volcanic hazards to coastal areas adjacent to the volcano with the resulting tsunami severely devastated the entire coasts of Sunda Strait. The source and time propagation of the tsunami have been in debate based on analysis of pyroclastic deposits, tide and pressure gauge records. Field evidence from submarine volcaniclastic deposits around the volcano showed that the great 1883 eruption and tsunami were directly connected to such flows pouring the strait on 26-27 August 1883. Recognition of this source mechanism of volcanic tsunamis is of primary significance in regions, where pyroclastic flows produced by explosive eruption of an active volcano may be discharged into the nearby ocean waters.

The rise and gravitational collapse of the crater in underwater 'natural' explosions create two successive bores followed by a number of smaller undulations propagating radially outward from the source. The initial surface displacement can be estimated as a function of the explosion energy at a given depth. Waves caused by underwater explosions usually have small amplitudes, relatively compared to those generated by tectonic earthquakes. Underwater explosions generate dispersive, short-period waves with the limited impact for the far-field. However, the effect of dispersion is reduced for underwater explosions occurring in shallow lakes, such as a tsunami wave with high run-ups at Karymsky Lake, Kamchatka, Russia in 1996. Nevertheless, hazards related to underwater explosions are unpredictable, leaving coastal communities nearby at risk.

A long-period ocean surface wave can also be possibly produced by phase-coupling with atmospheric shock waves but this phenomenon, the so-called meteo-tsunami requires certain conditions to set up. For an explosive eruption from an active submarine volcano, the air pressure must be high enough to excite free waves in the atmosphere, as observed during the Hunga Tonga-Hunga Ha'apai (HTHH) volcano eruption on 15 January 2022.

The transfer of energy from air to ocean waters works only on a deep and long stretch of the ocean surface. This is why the coupled air pressure-ocean water waves could explain the worldwide travelling tsunami recorded after the 1883 huge explosion of Krakatau but not the 15-30 m high waves observed in Sunda Strait that were most probably related to pyroclastic flows. A similar situation was then also observed in the Pacific Ocean during the 2022 HTHH huge explosion that was followed by a tsunami. In the HTHH aftermath, the early arrival of the small amplitude-leading ocean waves before the primary tsunami revealed the atmosphere-ocean dynamic coupling in the Pacific. This coupling produced unusual, fast-travelling transoceanic tsunami waves.

Lynett et al. (2022) reported the case of the 2022 HTHH huge explosive eruption, where the eruption generated tsunamis through at least doubly connected mechanisms, namely (1) air-sea coupling with the initial and powerful atmospheric shock waves radiating out from the explosion in the immediate vicinity of the volcano and (2) air-sea coupling with the air-pressure pulses that circled the Earth several times, leading to a global travelling, fast-moving meteo-tsunami. In the near field, tsunami propagation is mainly controlled by the eruptive event whereas in the far-field, the propagation is largely influenced by the Lamb atmospheric wave. We leave the detailed properties of the 2022 HTHH event for Chapters Four and Five.

Large explosive eruptions often result in the collapse of the central part of the edifice, thereby forming a caldera. In the case of underwater eruptions, the collapse of a caldera (see Figure 2.5) generates a subsidence of the water surface that initiates the propagation of a trough-leading wave. The size of the water subsidence depends on the geometry and time duration of the collapse, keeping in mind that large collapse lasting a few minutes is theoretically tsunamigenic but probably unrealistic. Whilst, in some circumstances sudden caldera collapse of a submarine volcano would produce significant wave heights on the surrounding shorelines.

However, determining the primary source mechanism of tsunamis generated during caldera-forming eruptions is frequently problematic as different tsunamigenic processes might play a role, such as volcano-tectonic earthquakes, slope instabilities, pyroclastic flows, underwater explosions, and atmospheric shock waves. Thus, it is difficult to say that a particular volcanic tsunami is sourced from a single generation mechanism except in some cases where post-event records from field surveys are available for comparison. For example, the computed tsunami heights generated by simulated pyroclastic flows in modern era are consistent with historical records of the 1883 Krakatau tsunami event in Sunda Strait. Other mechanisms, such as underwater explosion and caldera collapse do not fit with measurements of surface water level by tide gauges placed at Tandjung Priok, Jakarta.

One of the lessons learned from the 2018 Sunda Strait tsunami is that volcanic islands are commonly densely populated or close to populated coastlines. Hence, tsunami risk to nearby communities in the islands is relatively high. Thus, the Indonesian agencies have installed multiple early warning in tsunami-prone areas in Indonesian territory. The latest system would detect any disturbance on the water surface, including changes in the sea level caused by volcanic activity or submarine landslide.

2.4 Exercises

Answer clearly to the following questions regarding the content of Chapter Two.

1. Describe briefly some potential sources associated with tsunami generation.
2. Describe the principal differences in mechanisms and corresponding consequences between subaerial landslide-tsunamis and submarine landslide-tsunamis ?
3. Explain why it is hard to determine the exact source mechanism of tsunami excitation in cases of tsunamis triggered by volcanic processes.
4. According to your understandings, what are the principal differences in the source mechanism between the 2018 Palu Bay tsunami and the 2018 Sunda Strait tsunami ?
5. What makes different between the 2022 Hunga Tonga-Hunga Ha'apai tsunami and the 1883 Krakatoa tsunami ? What makes them similar anyway ?

This page is intentionally left blank

Chapter Three

TSUNAMI PROPAGATION SPEED

In general, a tsunami is a series of surface gravity waves, travelling on the ocean surface at the speed of 720-800 km/h and a corresponding wavelength of order 100 km or more. Destructive tsunami waves can be generated by both tectonic and non-tectonic scenarios, some of them are earlier discussed in Chapter Two (tectonic earthquakes, subaerial and submarine landslides, volcanic eruptions). Two notable recent tsunami occurrences are the 2018 Palu Bay tsunami, where the multiple sources of the strong ground motion and the submerged landslide just outside and inside the bay caused local tsunami excitation; it was about three months later, the 2018 Sunda Strait volcanic tsunami occurred, where the partially submerged landslide due to a slope instability of Anak Rakata led to a south-west flank failure of the volcano and in turn triggered a regional tsunami.

While a zone of generation is usually studied by a source model for tsunami generation, travelling tsunamis along a propagation zone are frequently approximated for a first look by shallow water, leading to the long wave speed formulation. Geophysical disturbances driven by internal and external sources during tsunami propagation in the open ocean may cause speed reduction. This chapter discusses the details of approximation usually used to derive a tsunami speed and the effects of both internal and external sources on the reduced speed. Particular attention is given to the effects of seafloor deformation and varying water density on the propagation.

3.1 Governing Equations

The underlying physics related to tsunami propagation is geophysical fluid dynamics. This discipline examines naturally occurring, large-scale flows (liquid and gas) on Earth. Thus, geophysical fluid dynamics discusses fluid dynamics at large scales. In this context, the cornerstone of fluid dynamics is the governing equations, comprising the continuity, momentum and energy equations. In their basic forms, these equations speak physics of fluid motion through a set of mathematical expressions written for three fundamental principles of physics on which fluid dynamics is based, namely (1) mass conservation; (2) the Newton's second law of motion; and (3) energy conservation. This section is thus devoted to derive briefly and discuss these equations.

3.1.1 Flow Model of the Fluid Motion

Before we proceed the complete form of the governing equations, it is better to start with fundamental mechanisms how physics principles are applied to a suitable flow model, describing a particular phenomenon in nature. Keep in mind that if any rigid body is in translational motion, the velocity of each part of the body is the same. But, if a fluid is in motion, the velocity may vary with particle's locations with respect to the basin in which the fluid is placed. Perhaps, at a small scale there exists some fluid's particles that are in circular motions even though the whole body of the fluid is in a translational motion. How do we describe a moving fluid so as to apply the fundamental physic principles using a suitable model of the flow ? For mechanics of a continuum fluid, the following choices, as shown in Figure 3.1 below, provide the answer to such a question.

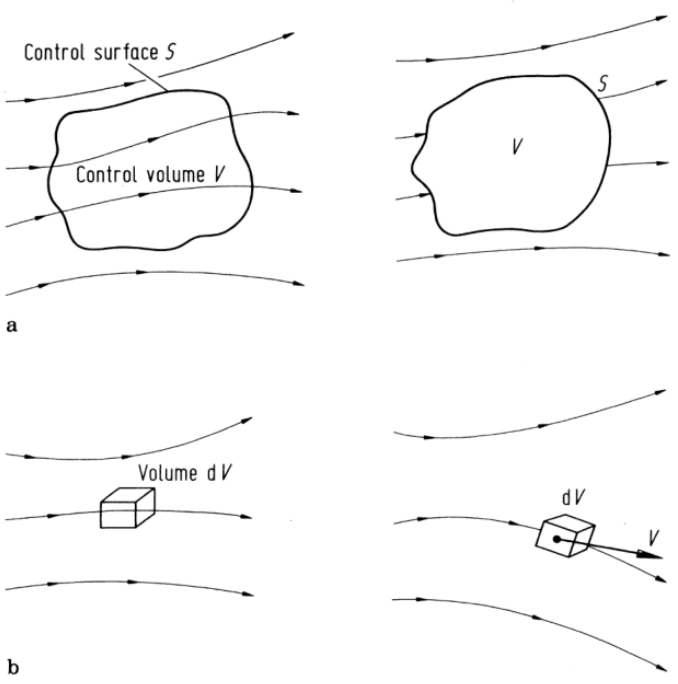

Figure 3.1. Diagram showing a model of the flow field using an approach of a finite control volume in (a) and an infinitesimal moving fluid element in (b) (taken from Chapter Two of Computational Fluid Dynamics, 3rd ed. by JD Anderson Jr, 2009).

Consider a general flow field as illustrated by the streamlines and a control volume V within a finite region of the flow bounded by a control surface S. The control volume is fixed in space with the fluid moving through it, as depicted by the left illustration in Figure 3.1(a). Alternatively, the control volume is moving with the fluid, as depicted by the right illustration in Figure 3.1(a), such that the same particles are always inside it.

The fundamental physics principles can be applied to the fluid inside the control volume and to the fluid crossing the control surface (if the control volume is fixed in space). Hence, with the control volume model we limit attention to the fluid in the finite region. The fluid flow equations are normally in integral forms, which can be converted to obtain the associated partial differential equations using an infinitesimally small fluid element, as seen in Figure 3.1(b). The equations obtained from the finite control volume fixed in space in either integral or partial differential forms are known as the conservation form of the governing equations. Whilst, the equations obtained from the finite control volume moving with the fluid flow in either integral or partial differential forms are referred to as the non-conservation form of the governing equations.

3.1.2 Material Derivative

Before deriving the governing equations required to describe tsunami dynamics, we need to understand mathematical expressions commonly used for fluid motion description, namely material derivative. This sub-section mainly emphasises on the physical meaning of material derivative and its role in the description of the flow. We begin discussions with choosing the model seen on the right of Figure 3.1(b), namely an infinitesimally small fluid element moving with the flow. Assuming that the fluid element is moving in a three-dimensional space of the cartesian system, we then have for the velocity field **u** as follows,

$$\mathbf{u} = u\hat{\imath} + v\hat{\jmath} + w\hat{k} \tag{3.1}$$

where u, v and w are components of the flow field with respect to x, y and z axes, respectively.

When a fluid element moving with the flow from one location to another in a cartesian space, we can then obtain 'material derivative' in its scalar form as follows,

$$\frac{d}{dt} = \frac{\partial}{\partial t} + u\frac{\partial}{\partial x} + v\frac{\partial}{\partial y} + w\frac{\partial}{\partial z} \tag{3.2}$$

Using $\nabla = \hat{\imath}\ \partial/\partial x + \hat{\jmath}\ \partial/\partial y + \hat{k}\ \partial/\partial z$, we can rewrite Eq. (3.2) as

$$\frac{d}{dt} = \frac{\partial}{\partial t} + \mathbf{u}.\nabla \tag{3.3}$$

The first term on the right-hand side of Eq. (3.3) is called 'local derivative', physically described as the time rate of change of any physical quantity at a fixed point in space and the second term is called 'convective derivative', physically described as the time rate of change of any physical quantity owing to the moving fluid element from one location to another in the flow field. Therefore, Eq. (3.3) represents a mathematical expression for

the material derivative differential operator, which is independent of coordinate systems. For example, if a scalar density field ρ as a function of space and time simply written as $\rho = \rho(x, y, z, t)$ follows the fluid motion, we can then write

$$\frac{d\rho}{dt} = \frac{\partial \rho}{\partial t} + u\frac{\partial \rho}{\partial x} + v\frac{\partial \rho}{\partial y} + w\frac{\partial \rho}{\partial z} \tag{3.4}$$

or in a scalar notation,

$$\frac{d\rho}{dt} = \frac{\partial \rho}{\partial t} + \mathbf{u}.\nabla\rho \tag{3.5}$$

In Eqs. (3.4) and (3.5), the material derivative operator $\frac{d}{dt}$ seen on the left-hand sides has the same meaning as a 'total derivative' with respect to time.

3.1.3 The Continuity Equation

Here we apply the physics principle of mass conservation (even if the case considered is fluid motion) to both the finite control volume and infinitesimal fluid element models of the flow. In a bit detail, we choose the finite control volume to be fixed in space, as seen on the left side of Figure 3.1(a) while the infinitesimal fluid element will be moving with the flow, as shown on the right side of Figure 3.1(b). In this way, we are going to compare the continuity equation derived for the conservation and non-conservation forms.

First, consider a finite control volume model fixed in space for the flow on the left side of Figure 3.1(a). Then, we set up a balance between the rate at which the fluid flows in and out of the control volume through a simple statement of qualitative mass conservation within the control volume,

$$\left\{\begin{array}{l}\text{Net mass flow } \textit{out}\\ \text{of control volume}\\ \text{through surface } S\end{array}\right\} = \left\{\begin{array}{l}\text{time rate of decrease}\\ \text{of mass inside control}\\ \text{volume}\end{array}\right\}$$

After some mathematical steps, we obtain

$$\frac{\partial}{\partial t}\int_V \rho\, dV = -\oint_S \rho\mathbf{u}.d\mathbf{S} \tag{3.6}$$

where on left side is volume integral and on the right side is closed surface integral. Equation (3.6) is termed as the integral form of the continuity equation (note that this equation is also called conservation form). The finite control volume is arbitrarily drawn in space and thus it can be converted into its associated differential form as follows,

$$\frac{\partial \rho}{\partial t} + \nabla.(\rho\mathbf{u}) = 0 \tag{3.7}$$

Equation (3.7) represents the continuity equation in its conservation form.

Here we note the following steps to complete: (1) by applying the finite control volume model, we have obtained the continuity equation, as seen in Eq. (3.6) in integral form; (2) after some mathematical manipulation, we have obtained the continuity equation in a partial differential form, as written in Eq. (3.7); and (3) by selecting the fluid flow model to be fixed in space, we have obtained the conservation form of the continuity equation.

Now, consider the moving fluid element model, as seen on the right side of Figure 3.1(b). Since mass is always conserved, we can state that the time rate of change of the mass of the fluid element is zero as the fluid element moves along with the flow. Using definition of $\nabla . \mathbf{u}$ in the cartesian system, we can then write

$$\frac{d\rho}{dt} + \rho \nabla . \mathbf{u} = 0 \tag{3.8}$$

Equation (3.8) is thus the continuity equation in a non-conservation form. In the same manner as previously written, the following steps to finish are as follows: (1) by applying the infinitesimal fluid element model, we have obtained Eq. (3.8) in partial differential form; and (2) by choosing the fluid model to be moving with the flow, we have obtained the non-conservation form of the continuity equation.

Equations (3.7) and (3.8) represent mass conservation in the form of partial differential equations for the conservation and non-conservation forms, respectively. Both equations are equally valid with one equation can be obtained from the other. Using this identity

$$\nabla . (\rho \mathbf{u}) = \rho \nabla . \mathbf{u} + \mathbf{u} . \nabla \rho \tag{3.9}$$

and substituting Eq. (3.9) into Eq. (3.7) yield,

$$\frac{\partial \rho}{\partial t} + \mathbf{u} . \nabla \rho + \rho \nabla . \mathbf{u} = 0 \tag{3.10}$$

The first two terms on the left side of Eq. (3.10) are the material derivative of the density field, as given in (3.5). Therefore, Eq. (3.10) can be further written to have the same form as Eq. (3.8), which is the non-conservation form of the continuity equation. The term $\frac{d\rho}{dt}$ is the time rate of change of density following the moving fluid element. It can be non-zero because of changes in pressure, temperature, or composition (such as, salt content in ocean waters or salinity). Nevertheless, liquids are almost incompressible and hence the incompressible assumption of ocean waters is good approximation.

For steady flows, where the density is time independent and the fluid is incompressible, meaning that the density remains constant following the fluid motion or mathematically $\frac{d\rho}{dt} = 0$, then the remaining part of the continuity equation is as follows,

$$\nabla . \mathbf{u} = 0 \tag{3.11}$$

or in scalar notation,

$$\frac{\partial u}{\partial x}+\frac{\partial v}{\partial y}+\frac{\partial w}{\partial z}=0 \tag{3.12}$$

Equation (3.12) reads as follows: mass conservation will lead to volume conservation for steady flows and incompressible fluids. The insignificance of $\frac{d\rho}{dt}$ in the equation of continuity given in Eq. (3.8) is part of simplifications under the Boussinesq fluids.

3.1.4 The Momentum Equation

In this sub-section, we again apply physics principle to the moving fluid element model, as shown on the right of Figure 3.1(b), in such a way that makes everything easy to write and understand with no physics concept being left. To start with, let us examine simple illustration of the net force acting on a body of an infinitesimal moving fluid element, as depicted in Figure 3.2 below.

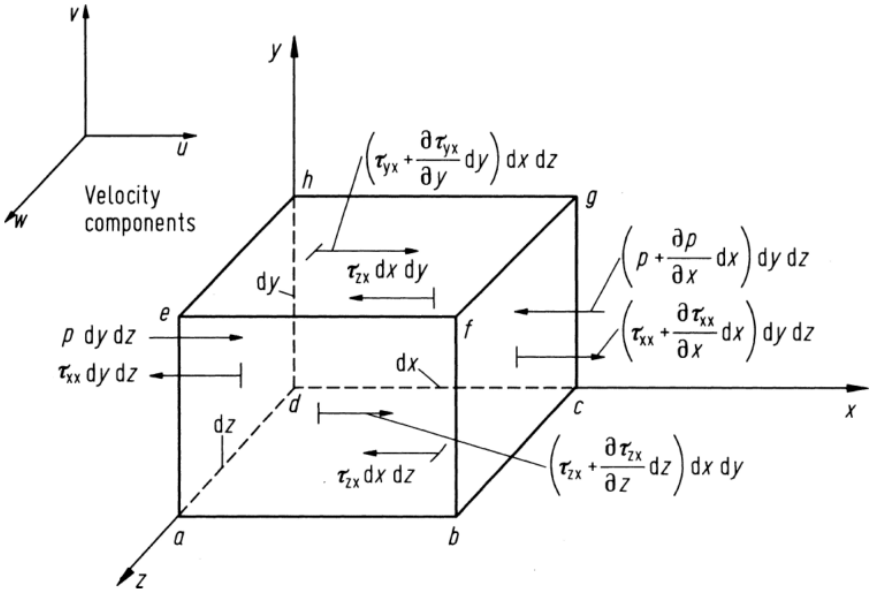

Figure 3.2. Sketch showing an infinitesimally small, moving fluid element with only the forces in the x-direction being illustrated (taken from Chapter Two of Computational Fluid Dynamics, 3rd ed. by JD Anderson Jr, 2009).

The Newton's second law of motion states that the net force acting on the fluid element equals the mass of the element times the element acceleration. This statement is actually a vector relation hence can be split into three scalar relations along the x, y, and z-axes. The net force is the sum of all body and surface forces. The body forces are here acting upon the volumetric mass of the fluid element, for example, gravitational, electric and

magnetic forces. Whilst, the surface forces are acting on the surface of the fluid element, including the distributions of pressure, normal and shear stresses acting on the surface. In this context, the normal and shear stresses are related to the time rate of change of the deformation of the fluid element owing to the surface forces acting on it. The scalar notation of the Newton's second law of motion for the moving fluid element are

$$\rho \frac{du}{dt} = -\frac{\partial p}{\partial x} + \frac{\partial \tau_{xx}}{\partial x} + \frac{\partial \tau_{yx}}{\partial y} + \frac{\partial \tau_{zx}}{\partial z} + \rho f_x \tag{3.13}$$

$$\rho \frac{dv}{dt} = -\frac{\partial p}{\partial y} + \frac{\partial \tau_{xy}}{\partial x} + \frac{\partial \tau_{yy}}{\partial y} + \frac{\partial \tau_{zy}}{\partial z} + \rho f_y \tag{3.14}$$

$$\rho \frac{dw}{dt} = -\frac{\partial p}{\partial z} + \frac{\partial \tau_{xz}}{\partial x} + \frac{\partial \tau_{yz}}{\partial y} + \frac{\partial \tau_{zz}}{\partial z} + \rho f_z \tag{3.15}$$

where $\frac{\partial p}{\partial x}$, $\frac{\partial p}{\partial y}$ and $\frac{\partial p}{\partial z}$ are the pressure gradients and f_x, f_y and f_z are the body forces along the three cartesian axes, respectively. Equations (3.13), (3.14) and (3.15) are known as the momentum equation in non-conservation forms, and frequently called a set of Navier-Stokes equations. These equations can also be converted into conservation forms. Detailed conversion is left for the reader, we here provide the final results only,

$$\frac{\partial \rho u}{\partial t} + \nabla.(\rho u\, \mathbf{u}) = -\frac{\partial p}{\partial x} + \frac{\partial \tau_{xx}}{\partial x} + \frac{\partial \tau_{yx}}{\partial y} + \frac{\partial \tau_{zx}}{\partial z} + \rho f_x \tag{3.16}$$

$$\frac{\partial \rho v}{\partial t} + \nabla.(\rho v\, \mathbf{u}) = -\frac{\partial p}{\partial y} + \frac{\partial \tau_{xy}}{\partial x} + \frac{\partial \tau_{yy}}{\partial y} + \frac{\partial \tau_{zy}}{\partial z} + \rho f_y \tag{3.17}$$

$$\frac{\partial \rho w}{\partial t} + \nabla.(\rho w\, \mathbf{u}) = -\frac{\partial p}{\partial z} + \frac{\partial \tau_{xz}}{\partial x} + \frac{\partial \tau_{yz}}{\partial y} + \frac{\partial \tau_{zz}}{\partial z} + \rho f_z \tag{3.18}$$

Equations (3.16), (3.17) and (3.18) are called the Navier-Stokes equations in conservation forms. The Navier-Stokes equations in both non-conservation (Eqs. 3.13, 3.14, 3.15) and conservation (Eqs. 3.16, 3.17, 3.18) forms provide the detailed description of all forces acting on the fluid, but in some sense they are written in complex mathematical symbols. In the following paragraphs, however, we simplify them using vector notation and show that the importance of the Boussinesq approximation.

Back to the Navier-Stokes equations in the non-conservation forms, as previously given in Eqs. (3.13), (3.14) and (3.15). These equations hold for problems in hydrodynamics either fluids in the deep or near and at the surface (for example: the lakes, the oceans) and those in the layered atmosphere at any scale of motion. In the vector notation, such equations can be written as

$$\rho \frac{d\mathbf{u}}{dt} = -\boldsymbol{\nabla} p + \rho \mathbf{f}_b + \mu \nabla^2 \mathbf{u} \tag{3.19}$$

where μ represents the dynamic viscosity of the fluid, $\mathbf{f}_b$ denotes the total body forces over the mass of the fluid. Equation (3.19) is in its general form. For inviscid fluids with $\mu = 0$, it follows that viscous effects are negligible, generally found to be true if it is far from boundaries of the flow field. For example, flowing ocean waters in the open ocean are influenced by the local gravity $\mathbf{g}$ as the only body force. In such a case, then Eq. (3.19) becomes

$$\rho \frac{d\mathbf{u}}{dt} = -\nabla p + \rho \mathbf{g} \tag{3.20}$$

In practice, Eq. (3.20) can be further simplified regarding an internal factor sourced from tsunami wave characteristics, for instance wavelength, and an external factor sourced from ocean basin, for instance water depth. The ratio between these factors is important to distinguish whether deep water or shallow water approximation is used to describe tsunami dynamics. Details of these approximations are discussed in next sections.

Now, let us consider a hypothetical static reference state in which the density field is given by ρ_o everywhere (with ρ_o is the mean density) and the pressure field is given by $p_o(z)$ so that $\nabla p_o = \rho_o \mathbf{g}$ (with p_o is the mean pressure). Subtracting this relation from Eq. (3.20) and writing $p = p_o + p'$ and $\rho = \rho_o + \rho'$ where p' and ρ' are small variations in p_o and ρ_o such that $p' \ll p_o$ and $\rho' \ll \rho_o$, respectively, we obtain

$$\rho \frac{d\mathbf{u}}{dt} = -\nabla p' + \rho' \mathbf{g} \tag{3.21}$$

Then dividing Eq. (3.21) by ρ_o at the first chance, we obtain

$$\left(1 + \frac{\rho'}{\rho_o}\right) \frac{d\mathbf{u}}{dt} = -\frac{1}{\rho_o} \nabla p' + \frac{\rho'}{\rho_o} \mathbf{g} \tag{3.22}$$

The ratio of ρ'/ρ_o appears in both the inertia $d\mathbf{u}/dt$ on the left side of Eq. (3.22) and the buoyancy $\mathbf{g}$ terms on the right side of Eq. (3.22). For fluids with small values of ρ'/ρ_o, the density variations generate only a small correction to the inertia term and hence can be neglected. However, the buoyancy term $\mathbf{g}\,\rho'/\rho_o$ on the right side is very important and hence cannot be neglected. For example, it is true that the density variations drive convective motion when a layer of fluid is vertically heated. The magnitude of $\mathbf{g}\,\rho'/\rho_o$ is the same order as the vertical acceleration or the viscous term. We then conclude that the density variations are ignored relative to other terms in the momentum equation, except when ρ is multiplied by $\mathbf{g}$. This statement shows the significance of the buoyancy or the buoyant force in the Boussinesq approximation for the horizontal component of the Navier-Stokes equations.

3.1.5 The energy equation

Similar to the previous sub-section, this sub-section also utilises an infinitesimally small, moving fluid element for an energy equation (see Figure 3.3). The physics principle to invoke is related to qualitative energy conservation along the small moving fluid element as follows,

$$\left\{\begin{array}{l}\text{Rate of change of}\\ \text{energy inside the}\\ \text{fluid element}\end{array}\right\} = \left\{\begin{array}{l}\text{Net flux of}\\ \text{heat into}\\ \text{the element}\end{array}\right\} + \left\{\begin{array}{l}\text{Rate of working done on}\\ \text{the element due to body}\\ \text{and surface forces}\end{array}\right\}$$

Here we are not going to show the derivation of the energy equation in details; rather, we will provide only the final results for both non-conservation and conservation forms, which hold for incompressible, inviscid fluids (the term 'fluids' here can be replaced with flows just because the topic under consideration is a moving fluid, such as ocean waters). Remember that, by definition, incompressible flows are flows having relatively small density variation while inviscid flows are flows, where dissipative, transport phenomena by viscosity, diffusion and thermal conductivity are ignored in the governing equations. The governing equations for unsteady, three-dimensional, incompressible, inviscid flows are then obtained by neglecting viscous terms as follows,

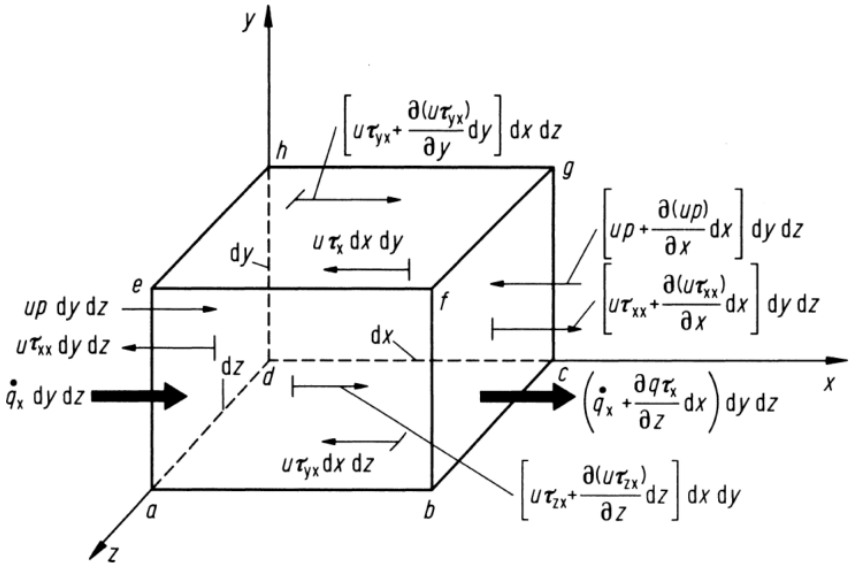

Figure 3.3. Sketch showing an infinitesimally small, moving fluid element with only the fluxes of energy in the x-direction being illustrated (taken from Chapter Two of Computational Fluid Dynamics, 3rd ed. by JD Anderson Jr, 2009).

In the non-conservation form, the energy equation takes the form of

$$\rho \frac{d}{dt}\left(e + \frac{\mathbf{u}.\mathbf{u}}{2}\right) = p\dot{q} - \frac{\partial(up)}{\partial x} - \frac{\partial(vp)}{\partial y} - \frac{\partial(wp)}{\partial z} + \rho \mathbf{f}.\mathbf{u} \tag{3.23}$$

and its counterpart, the conservation form of the energy equation is given by

$$\frac{\partial}{\partial t}\left[\left(e + \frac{\mathbf{u}.\mathbf{u}}{2}\right)\right] + \nabla.\left[\rho\left(e + \frac{\mathbf{u}.\mathbf{u}}{2}\right)\mathbf{u}\right] = p\dot{q} - \frac{\partial(up)}{\partial x} - \frac{\partial(vp)}{\partial y} - \frac{\partial(wp)}{\partial z} + \rho \mathbf{f}.\mathbf{u} \tag{3.24}$$

where e denotes the internal energy of the fluid element, $\dot{q}$ represent heat transfer by thermal conduction into the moving fluid element, and $\mathbf{f}$ is the body force acting upon the fluid element.

It is obvious that for both the momentum and energy equations, the difference between the non-conservation and conservation forms of the equations is just the left-hand side. The right-hand side of the equations in the two distinct forms is exactly the same. However, the momentum equation is normally written in vector notation, as given in Eqs. (3.19), (3.20) and (3.21) whereas the energy equation is given in scalar notation, as written in Eqs. (3.23) and (3.24).

3.2 Small-Amplitude Surface Gravity Waves

In this section, we will derive and discuss a specific class of waves of fundamental interest that serve as the underlying physics for tsunami dynamics in the ocean. These waves are called gravity waves, propagating at the ocean surface with relatively small amplitudes. The small-amplitude wave theory for two-dimensional, freely propagating, gravity waves is developed by linearising the equations defining the free surface and bottom boundary conditions. Determination of a velocity potential is performed to satisfy the requirements for irrotational flow that is valid throughout water column except at the boundary layers (at the air–water interface and the bottom). The potential is used to derive the equations defining various wave characteristics.

The required assumptions made available for the small-amplitude, surface gravity wave propagation theory are as follows:

- The ocean water is homogeneous, incompressible and inviscid.
- Surface tension forces are negligible hence no internal pressure or gravity waves affecting the flow.
- The flow is irrotational hence no shear stress at the air–sea interface (the free surface boundary) and the bottom (the rigid bottom boundary). Wind waves are not considered and the fluid particles slip freely at the bottom and other solid fixed

surfaces. Therefore, the velocity potential φ must satisfy the Laplace equation for two-dimensional flows as follows,

$$\frac{\partial^2 \varphi}{\partial^2 x} + \frac{\partial^2 \varphi}{\partial^2 z} = 0 \tag{3.25}$$

where, as usual, x and z are the horizontal and vertical coordinates, respectively.

- The bottom boundary is stationary, impermeable and horizontal. For surface gravity waves propagating along a sloping bottom boundary (when propagating toward shorelines in the nearshore), the waves can be simply accommodated by the assumption of a horizontal bottom if the slope is not too steep.
- The pressure along the air–sea interface (the free surface boundary) is constant. Thus, no pressure is exerted by the wind and the aerostatic pressure difference between the wave crest and trough is then negligible.
- The wave height H is relatively small compared to the wavelength L and the water depth $d + \eta \approx d$ (because $\eta \ll d$). As the fluid particle velocities are proportional to the wave height while the wave speed is related to the wavelength and the depth, the particle velocities are relatively small compared to the wave speed. This allows to linearise higher order free surface boundary conditions and apply this condition at the 'still' water level (being always horizontal) rather than at the water surface (moving up and down) to get an easier solution. It follows that the small-amplitude wave theory is most limited for high waves in deep and shallow waters. However, the small-amplitude wave theory remains important for wave analysis of tsunami propagation (see Figure 3.4 for detailed kinematic parameters of the wave).

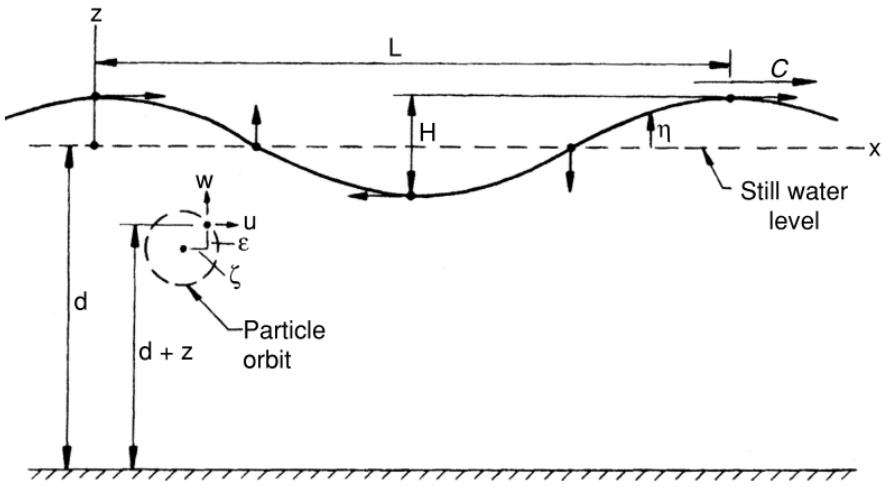

Figure 3.4. Sketch showing parameters involved in propagating surface gravity waves (taken from Chapter Two of Basic Coastal Engineering, 3rd ed. by RM Sorensen, 2006).

Figure 3.4 shows a surface gravity wave traveling at a phase speed c on water depth d in the x-z coordinate system. The x axis is the still water level position and the bottom is at $z = -d$. The wave surface profile is defined by $z = \eta(x, t)$, where η denotes vertical surface elevation measured from the still level, which is a function of x and t.

The small-amplitude wave theory is here developed by solving the Laplace Eq. (3.25) for the sketch depicted in Figure 3.4 with the appropriate free surface and bottom boundary conditions. At the bottom there is no normal flow, resulting in the bottom boundary condition as follows,

$$w = \frac{\partial \varphi}{\partial z} = 0 \quad \text{at } z = -d \tag{3.26}$$

whereas at the free surface there is a kinematic boundary condition, relating the vertical component of the particle velocity at the surface to the surface position as follows,

$$w = \frac{\partial \eta}{\partial t} + u\frac{\partial \eta}{\partial x} \quad \text{at } z = \eta \tag{3.27}$$

The Bernoulli equation for unsteady irrotational flow can be written as follows,

$$\frac{1}{2}(u^2 + w^2) + \frac{p}{\rho} + gz + \frac{\partial \varphi}{\partial t} = 0 \tag{3.28}$$

where g is the gravitational acceleration, p is the pressure field, and ρ is the fluid density. At the water surface where the pressure field is zero, the dynamic boundary condition takes the form of

$$\frac{1}{2}(u^2 + w^2) + gz + \frac{\partial \varphi}{\partial t} = 0 \quad \text{at } z = \eta \tag{3.29}$$

Both the kinematic and dynamic boundary conditions have to be linearised and applied at the still level rather than at the water surface. As a result, we have both conditions in two consecutive equations below,

$$w = \frac{\partial \eta}{\partial t} \quad \text{at } z = 0 \tag{3.30}$$

and

$$g\eta + \frac{\partial \varphi}{\partial t} = 0 \quad \text{at } z = 0 \tag{3.31}$$

Having employed the Laplace Eq. in (3.25), the boundary conditions in (3.26) and (3.27), and the linearised boundary conditions in (3.30) and (3.31), we can derive the velocity potential for the small-amplitude wave theory with its most useful form as follows,

$$\varphi = \frac{gH}{2\omega}\frac{\cosh k(d+z)}{\cosh kd}\sin(kx - \omega t) \tag{3.32}$$

where ω is the angular frequency. Since the wave length L or wave number k depends upon the wave period T and water depth d, when the wave height H, the wave period T and the water depth d are known, the wave is fully defined. When these conditions are satisfied, all the wave characteristics, including vertical displacement η of the surface elevation and the wave speed c can be determined. At this stage, we are ready to insert the velocity potential φ given in (3.32) into the linearised dynamic boundary condition written in (3.31) to obtain the vertical displacement η of water surface as follows,

$$\eta = \frac{H}{2}\cos(kx - \omega t) \tag{3.33}$$

or alternatively,

$$\eta = \frac{H}{2}\cos 2\pi\left(\frac{x}{L} - \frac{t}{T}\right) \tag{3.34}$$

Thus, the small-amplitude wave theory yields a function of a cosine water surface profile. The inherent problem is associated with increasing wave amplitudes the profile becomes vertically asymmetric with a more peaked wave crest and a flatter wave trough.

Now, with Eqs. (3.33) or (3.34) at hands we are ready to derive wave speed formulation by combining Eqs. (3.27) and (3.29) and eliminating the surface elevation to obtain

$$\frac{\partial^2\varphi}{\partial^2 t} + g\frac{\partial\varphi}{\partial z} = 0 \quad \text{at } z = 0 \tag{3.35}$$

Inserting the velocity potential φ given in Eq. (3.32) into Eq. (3.35), differentiating and rearranging it, we have the angular frequency in the form of

$$\omega^2 = gk\tanh kd \tag{3.36}$$

Using wave dispersive relation $c = \frac{\omega}{k}$ we can write the speed of the small-amplitude, surface gravity wave as follows,

$$c = \sqrt{\frac{gL}{2\pi}\tanh\frac{2\pi d}{L}} \tag{3.37}$$

Equation (3.37) shows that the speed of the small-amplitude, surface gravity waves is independent of H. Instead, it depends on L (or frequency, for which it is frequently called the speed of dispersive waves) and the ratio of d/L (for which the relative amount of external to internal measures is of significance). Here, we use the terms 'wave steepness' defined as the wave height divided by the wave length: H/L and 'relative depth' defined as the water depth divided by the wave length: d/L. Regarding tsunami propagation in the ocean, the relative depth d/L is crucial as it determines whether the propagation is classified into deep water or shallow water waves.

In the context of surface gravity waves, Eq. (3.37) reads in a different manner as follows: for a particular depth, the wave propagates faster with increasing wavelength. However, for a given wavelength, the waves in deeper waters travel at a larger phase speed than in shallower waters. In the context of tsunami propagation, effects of wave dispersion are larger with increasing travel time and travel distance. Although frequency dispersion is frequently ignored in earthquake-induced tsunamis, it may be important particularly for distant observations from the source area (Glimsdal et al., 2013). Dispersion effects on deep-water propagation is mostly noticeable for trans-oceanic tsunamis, for example, the 2004 Indian Ocean, the 2010 Maule, Chili and the 2011 Tohoku, Japan tsunamis.

3.2.1 Deep-Water Approximation

Deep-water approximation mainly relies on a mathematical simplification where $d \gg L$ in Eq. (3.37) such that a factor of $\frac{2\pi d}{L}$ becomes large enough, leading to $\tanh\frac{2\pi H}{\lambda} \approx 1$. Hence, Eq. (3.37) changes into

$$c = \sqrt{\frac{gL}{2\pi}} \tag{3.38}$$

In other words, Eq. (3.38) is considered a special case of Eq. (3.37) for freely travelling, small-amplitude, surface gravity waves at all depths. It is independent of the water depth. Figure 3.5 below shows circular orbital motion of the fluid particle at a small scale within a surface gravity wave travelling in the deep-water approximation.

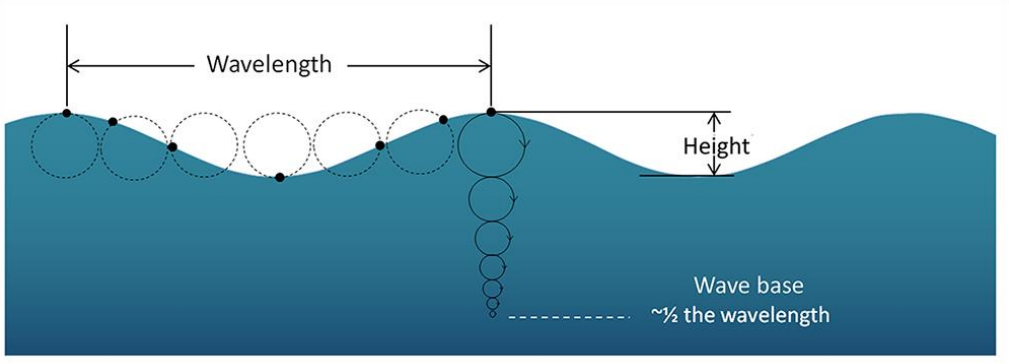

Figure 3.5. Sketch showing orbital motion of a fluid particle within a travelling gravity wave, extending down to the wave base at a depth of approximately half of the wavelength (taken from https://rwu.pressbooks.pub/webboceanography/chapter/10-1-wave-basics/).

As illustrated, the size of the orbital motion decreases with water depth as the wave has less effects on deeper water, indicated by smaller diameters of the orbits in deeper layers.

Eventually, at some depth there is no more circular movement and the water is effectively unaffected by the surface wave action. This depth is termed the wave base, equivalent to a half of the wavelength. Since the wavelengths of most ocean water waves are less than a few hundred meters, most deeper layers of the ocean are unaffected by surface waves (but this is not the case for tsunamis in which the entire water column is influenced). When the water below the water waves is deeper than the wave base, such waves are called deep water waves. Most ocean gravity waves are classified into deep water waves. These waves experience no interference with topography hence the wave speed depends on the wavelength only, as seen in Eq. (3.38). However, for ease most tsunami modelling relies much on a set of shallow-water equations for examination of tsunami dynamics in both propagation and mitigation zones (for example, determination of travel times and hence arrival times, and run-ups).

3.2.2 Shallow-Water Approximation

In this sub-section, we discuss shallow-water approximation for the small-amplitude, surface gravity waves. In contrary to the deep-water case, the shallow-water assumption is made available for $d \ll L$ such that a factor $\frac{2\pi d}{L}$ becomes small enough, leading to $\tanh\frac{2\pi d}{L} \approx \frac{2\pi d}{L}$. Thus, Eq. (3.37) changes into

$$c = \sqrt{gd} \tag{3.39}$$

Equation (3.39) is frequently applied to the case where the horizontal length scale L is much greater than the vertical length scale d. Under this condition, conservation of mass (or more precisely volume conservation for two dimensional flows given in Eq. (3.12)), implies that the vertical velocity w is small compared to the horizontal velocity u such that the horizontal gradient of the horizontal velocity is then proportional to (but it is in the opposite value) the vertical gradient of the vertical velocity. It can also be shown from the momentum equation in Eq. (3.20) that the vertical pressure gradient is hydrostatic and the horizontal velocity field is constant throughout the depth. It is easy to understood that shallow-water models are simultaneous non-linear partial differential equations, representing conservation of mass, momentum and energy, as previously explained in §3.1. In some circumstances the non-linear terms can be deleted from the equations.

In natural situations, the horizontal length scale is common to be much greater than the vertical length scale. It follows that the shallow-water approximation is widely applicable to fluid dynamics at all scales of motion, including most atmospheric and oceanic flows.

The shallow-water approximation is commonly used to describe the flow of water waves in the oceans, coastal seas and estuaries. Such approximation is used to predict the wave velocity and wave height at varying locations within a region of interest at different times. This is why many tsunami modelers have used this approximation to model tsunami waves for tsunami hazard analysis that is critical to large numbers of community at risk. In the context of tsunami propagation, Eq. (3.39) is frequently called the long wave speed since the wavelength of a tsunami wave in the open ocean can be 200 km long, compared to a typical ocean depth of only 5000 m deep, confirming $d \ll L$.

In addition to the difference formulas in the speed, shallow-water waves are different from deep-water waves in that the shallow-water waves interact with seafloor and hence part of the shallow-water waves near and at the surface are also influenced by bottom topography, making them having reduction in speed whenever they come onshore at relatively shallow depth, which will be discussed in details in Chapter Five. For now, it is enough to say that in the absence of geophysical disturbance in the ocean tsunami waves travel at a nearly constant value given by Eq. (3.39), the so-called long wave speed. Discussions on the speed in the presence of geophysical disturbance will be provided in Chapter Four.

3.3 Exercises

Answer clearly to the following questions regarding the content of Chapter Three.

1. Why do conservation of all mass, momentum and energy hold for tsunami wave propagation ?
2. What are the primary differences between the non-conservation and conservation forms of mass, momentum and energy conservation ?
3. What is the Boussinesq approximation for fluid motion ? Consider this statement as follows: “The ocean water is homogeneous, incompressible and inviscid”. Which one from such statement relevant to Boussinesq fluids ?
4. What are dispersive water waves ? Do you think that tsunami waves are dispersive or not ? Why do you think so ?
5. Why are so many tsunami modelers in demand for shallow-water approximation ?

Chapter Four

SPEED AND TIME MEASUREMENTS

This chapter deals with measurements (based on theoretical measures) of two kinematic quantities associated with tsunami propagation, namely speed and time measurements, and their corresponding impact on the propagation. These measurements have to be performed accurately enough for reliable tsunami modelling. It has been long known that tsunami wave propagation in the open ocean can be, to the first order, simulated using an approach of the shallow-water approximation, previously discussed in §3.2.2. This approximation has been successful to model the wave propagation in particular for travel distance within the range of the so-called near-fields. It follows that prediction of tsunami arrival times at near-field stations at varying locations based on travel times calculated using the standard theory of non-dispersive, long wave speed matches with time records obtained from direct observations by monitoring instrument. However, recent simulations of trans-oceanic tsunamis with travel distances exceeding thousands of kilometers have resulted in the apparent travel time differences between simulations (on the basis of long wave theory) and observations. It is the case with which this chapter is concerned.

4.1 Effect of Seafloor Deformation on Long Wave Speed

It has been widely known that the speed of 'conventionally travelling' tsunami waves is typically calculated using the shallow-water wave approximation over a rigid body Earth. This particular speed depends only on water depth (see again Eq. (3.39)), which is used by many tsunami modellers to model tsunami propagation. However, it has been noticed that far-field observations of tsunami waves (for which this is directly related to cases of trans-oceanic tsunamis), including the great events of the 2010 Maule, Chili and the 2011 Tohoku, Japan tsunamis, show systematic late arrivals of the waves in both events than expected from the standard long wave theory. The simulated travel times at far regions further than 10,000 km way from the source were found to be systematically shorter than those obtained from field observations by 15–20 minutes for the both tsunamis. These shed light on tsunami modelling to incorporate factors affecting tsunami propagation. For tectonic earthquake-generated tsunamis, the elasticity of the Earth that may lead to

seafloor deformation when the large events occur is the one, likely to be able to modify tsunami wave speeds. This section then provides basic physics principles of possible mechanisms of the delayed propagation hence the late arrivals found in the observations for reliable, advanced tsunami modelling.

Interactions between an elastic Earth at ocean bottom topography and a tsunami wave can be considered wave dispersion arising from the elastic seafloor deformation due to tsunami loading (Inazu and Saito, 2013). The bottom deformation produces feedback on tsunami spatial patterns that leads to the speed reduction and hence delayed arrivals of the wave. Figure 4.1 provides a simple sketch, illustrating a small change in the vertical displacement ($\eta - \eta_o$) of sea surface elevation owing to deformed sea bottom ($-\eta_o$) at the initial condition. Here, η is the water surface elevation at any time.

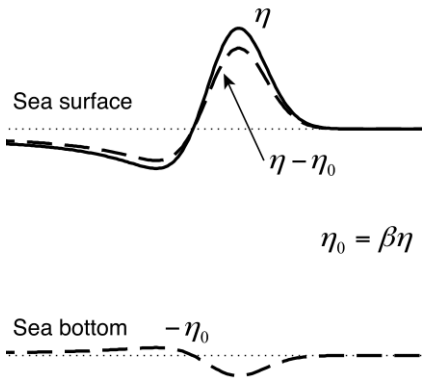

Figure 4.1. Sketch showing the effect of ocean self-attraction and loading or seafloor deformation loading on the water surface elevation (taken from Inazu and Saito, 2013).

Following Figure 4.1, the simplified governing equations for tsunami propagation with the inclusion of seafloor deformation effects are given by

$$\frac{\partial u}{\partial t} = -gd\frac{\partial}{\partial x}(\eta - \eta_o) \tag{4.1}$$

$$\frac{\partial \eta}{\partial t} + \frac{\partial u}{\partial x} = 0 \tag{4.2}$$

$$\eta_o = \beta\eta \tag{4.3}$$

where β is the constant parameter, describing the strength of the deformation effects, taken to be an empirically small value of up to 0.03. Equation (4.1) represents the one-dimensional momentum equation whereas Eq. (4.1) denotes the continuity equation and Eq. (4.3) is an additional equation, accommodating the effect of seafloor deformation. Let us now differentiate Eq. (4.2) with respect to time to obtain

$$\frac{\partial^2 \eta}{\partial t^2} + \frac{\partial}{\partial x}\frac{\partial u}{\partial t} = 0 \tag{4.4}$$

Substituting Eq. (4.1) into Eq. (4.4) yields

$$\frac{\partial^2 \eta}{\partial t^2} - gd\frac{\partial^2}{\partial x^2}(\eta - \eta_o) = 0 \tag{4.5}$$

which can be rewritten with the help of Eq. (4.3) as follows,

$$\frac{\partial^2 \eta}{\partial t^2} - gd(1-\beta)\frac{\partial^2 \eta}{\partial x^2} = 0 \tag{4.6}$$

Comparing Eq. (4.6) with standard wave equation as follows,

$$\frac{\partial^2 \eta}{\partial t^2} - c^2\frac{\partial^2 \eta}{\partial x^2} = 0 \tag{4.7}$$

we then obtain

$$c = \sqrt{gd}\,\sqrt{1-\beta} \tag{4.8}$$

for tsunami speed under influenced by seafloor deformation effects. Since β is definitely positive, then it is clear from Eq. (4.8) that the speed will be reduced to a smaller value than the long wave speed of 'conventional tsunamis' given in Eq. (3.39). The β factor that induces the reduced speed in Eq. (4.8) is the cause of tsunami late arrivals at far stations; it is useful to estimate time differences accounted for between simulated travel times and travel times recorded by monitoring instrument in the far-field regime.

A more detailed look at seafloor deformation effects is given by Tsai et al. (2013), where the aim is to examine factors that may affect the speed. The derivation devoted to account for the Earth elasticity rather than having a rigid ocean bottom is not provided here but the final result is as follows,

$$c = \sqrt{gd}\,\sqrt{1 - \frac{(1-\nu)\rho g}{\mu k}} \approx \sqrt{gd}\,\left[1 - \frac{(1-\nu)\rho g}{2\mu k}\right] \tag{4.9}$$

where ν is the Poisson's ratio of the elastic Earth, taken to be 0.3, μ is the shear modulus, taken to be 5×10^{10} Pa, ρ is the average density of sea water, taken to be 1036 kgm^{-3} and k is the wave number, taken to be $2\pi/1000$ km^{-1} (because the wavelength of tsunamis is assumed 1000 km). From these values, we can estimate the amount of reduced speed (measured in per cent) expected from taking into account the Earth elasticity, relative to the value predicted by the long wave speed given in Eq. (3.39). After simple calculation, we find a 1% reduction in the observed speed. Although this is a small reduction only, this speed correction is significant enough as it is larger than that given by the dispersive wave speed in Eq. (3.37). Note that the corrections given in Eqs. (4.8) and (4.9) have not yet considered the effects of ocean density stratification.

4.2 Effect of Stratified Density on Long Wave Speed

In the context of trans-oceanic tsunamis where travel distances can potentially exceed thousands of kilometers away, vertical density stratification (indicated by an increase in the density with depth) also results in a systematic correction for the speed reduction. This stratification is due to ocean water compressibility, which dominates over the effects of temperature and salinity on the density. According to Tsai et al. (2013), the key point to note in the examination of density stratification effect on the long wave speed written in Eq. (3.39) is that the pressure field remains hydrostatic while ocean water density increases linearly with water depth from the disturbed water surface according to

$$\rho(z') = \rho_o \left[1 + \rho_o g \frac{(d+\eta-z')}{\kappa}\right] \tag{4.10}$$

where z' is the height above the flattened sea bottom, ρ_o is the density at the surface, and κ is the bulk modulus (see Fig. 3.4 for the physical meanings of symbols d and η). Two other important definitions of water density relevant to the problem of interest are as follows,

$$\rho_d \approx \rho_o \left[1 + \rho_o g \frac{d}{\kappa}\right] \tag{4.11}$$

where ρ_d is the density at the bottom and

$$\rho_{\text{mean}} \approx \rho_o \left[1 + \rho_o \frac{d}{2\kappa}\right] \tag{4.12}$$

where ρ_{mean} is the mean density calculated from the sea bottom to the sea surface (see Fig. 4.1).

Using a combined form of Eqs. (3.39), (4.11) and (4.12), we can then derive (but detailed derivation is not provided here) the speed of tsunami waves under the influence of ocean stratification as follows,

$$c = \sqrt{gd}\sqrt{\frac{\rho_{\text{mean}}}{\rho_d}} \approx \sqrt{gd}\left(1 - \frac{\Delta\rho}{4\rho_{\text{mean}}}\right) \tag{4.13}$$

where $\Delta\rho = \frac{\rho_o^2 g d}{\kappa} \approx \rho_d - \rho_o$, representing the maximum difference between the bottom and surface water densities. For a typical ocean water with $d \approx 4000$ m (it is also possible to have $d \approx 5000$ m), $\rho_d \approx 1045$ kgm^{-3}, $\rho_o \approx 1026$ kgm^{-3} and $\rho_{\text{mean}} \approx 1036$ kgm^{-3} (integrated over the water column depth), we find that the value of c written in Eq. (4.13) is about 0.5% slower than the standard, shallow-water wave speed given by Eq. (3.39). It follows that the speed reduction due to ocean stratification is a half of that attributable to external geophysical disturbance, such as seafloor deformation given by Eq. (4.9).

In short, tsunami wave speed is reduced by the effects of the elasticity of the solid Earth in the form of seafloor deformation and the ocean water compressibility in the form of density-stratified ocean water. Hence, time delays during distant propagation recorded by monitoring instrument at far stations arise mostly from the seafloor deformation (external factor) and weakly from the stratified density (internal factor). The implication of these effects on tsunami travel time hence arrival time at varying locations is crucial for tsunami hazard analysis and the corresponding early warning for maximum safety. Therefore, the reduction in speed should be included in travel time computation for precise modelling of trans-oceanic tsunamis.

4.3 Tsunami Onset Time and Travel Time

By definition, tsunami onset time is associated with the moment at which a tsunami wave is induced by any source mechanism before travelling. In this context, a crucial question that may be raised at the first place is: How long does it take for a tsunami wave to be triggered after an earthquake striking ? The correct answer to such a question depends on earthquake source, such as the hypocentral and/or epicentre location and magnitude of the earthquake. Seismic signals from submarine earthquakes at shallow depths take shorter times to reach the surface hence may induce tsunamis immediately after the first ground motion. Large earthquakes with huge amounts of energy have larger chances to generate tsunamis within shorter times after the events. In general, a tsunami wave can be triggered within seconds or immediate times to several hours after an earthquake. However, it is important to keep in mind that not all, even underwater earthquakes result in tsunamis. Only earthquakes with large magnitudes where there is an abrupt change in ocean bottom topography that displaces a large volume of water column in the deep to the surface will produce a noticeable to destructive tsunami wave.

Tsunami travel time is defined as the time taken by a tsunami to travel from the source point where it is generated to a location recorded by instrument at a monitoring station. For practice observations, travel time is simply estimated using an approach of uniform motion for tsunami propagation and thus it is directly obtained from travel distance divided by tsunami speed. For this reason, discussions on tsunami speed are important; whether the speed is dispersive, which is a function of tsunami frequency or wavelength as well as water depth, as written in Eq. (3.37), or given in a much simple form but remaining dispersive for deep waters, as provided by Eq. (3.38), or depth-dependence only for shallow waters, as given by Eq. (3.39), well-known as the long wave speed.

Corrections to the long wave speed leading to adjustment to travel time measurements have been performed in response to the effects of the seafloor deformation with the speed is given by either Eq. (4.8) or Eq. (4.9) and the density stratification with the speed is given by Eq. (4.13). In tsunami modelling, travel time obtained using the long wave speed is called theoretical or estimated travel time while that derived from the reduced speeds is called observed travel time. The discrepancy between these values is of significance for tsunami hazard mitigation.

A map of estimated tsunami travel times to varying coastal locations worldwide derived for a particular event is usually provided by either relevant institutions, such as NOAA National Centers for Environmental Information (NCEI) or published work, as depicted in Fig. 4.2 below.

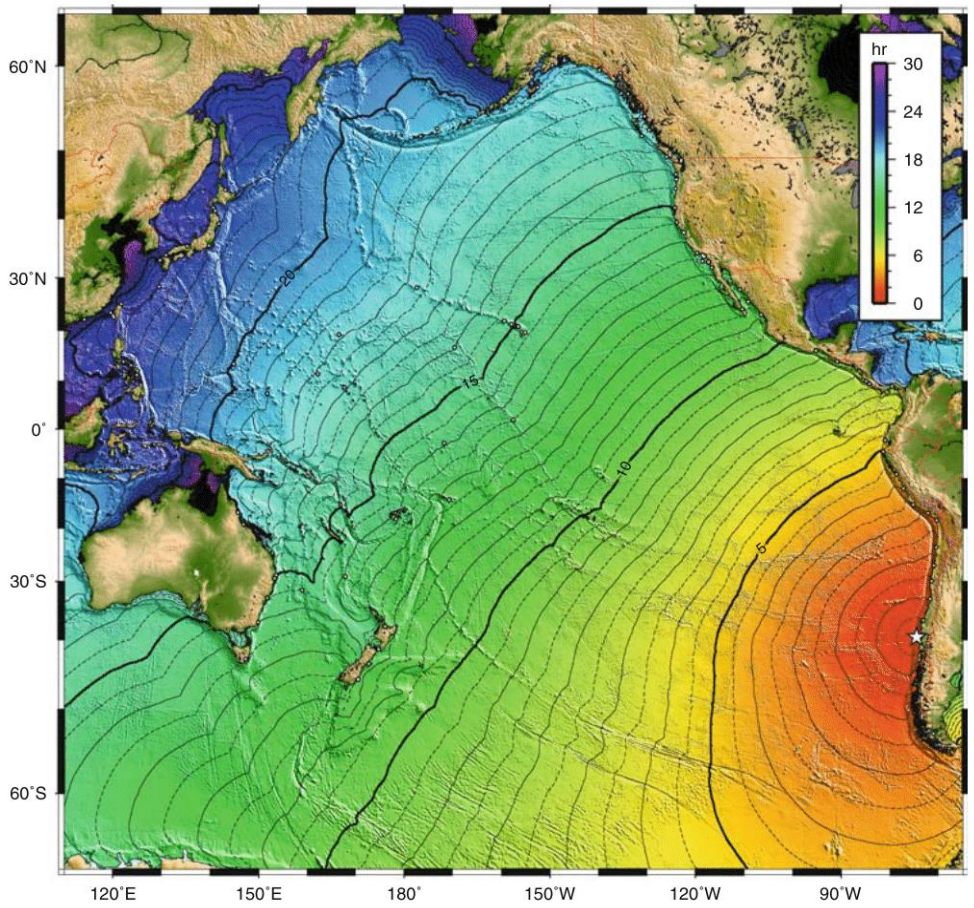

Figure 4.2. Estimated travel times for the Pacific basin-wide tsunami generated using tsunami simulation from the great 1960 Valdivia, Chile earthquake that in turn triggered a giant tsunami. White star shows the epicenter of the earthquake. Solid contours are hourly with a 30-minute interval, shown as dashed contours in between (taken from Wessel, 2009).

4.4 Tsunami Arrival Time and Time Delay

In theory, tsunami arrival time is expected to be the sum of tsunami onset time and estimated travel time. In practice, however, tsunami waves arrive late in particular at distant stations. This phenomenon suggests that tsunami time delays are present in far-field observations. Indeed, the discrepancy between the observed t_{obs} and estimated t_{est} travel times is accounted for the time delays Δt. In cases where $t_{\text{obs}} > t_{\text{est}}$ holds, leading to $\Delta t > 0$, the term 'delayed arrival' is correct.

$$\Delta t = t_{\text{obs}} - t_{\text{est}} \tag{4.14}$$

In many tsunami cases, such as the great 1960 Valdivia, Chilean earthquake-tsunami, scientific reports say that travel times obtained from field measurements were several to a few tens of minutes longer than those predicted by linear, long-period, shallow-water wave simulations. The delays in travel times hence arrival times have also been observed by tsunami monitoring instruments for two trans-oceanic tsunamis across the Pacific, such as, the 2010 Maule, Chili and the 2011 Tohoku, Japan events (see Fig. 4.3 in details). Systematic tsunami time delays of up to 15 minutes relative to the simulated long waves from the both events were reported (Watada et al., 2014). Tsunami waveforms based on observed travel times, taking the density stratification, the elastic solid Earth loading and geopotential perturbation into account were developed in comparison to those based on estimated travel times.

However, in a recent tsunami event dated on 15 January 2022, the Hunga Tonga-Hunga Ha'apai (HTHH) volcano in the south Pacific erupted and generated unusual tsunamis, with a unique, dual mechanism of dominance (see Fig. 4.4) associated with fast-traveling air-pressure pulses (atmospheric Lamb waves) originated from the explosive eruption. In the near-field, tsunami propagation is strongly controlled by the eruption, leading to a conventional tsunami travelling on the ocean surface at the long wave speed of about 220 ms^{-1} or 800 kmh^{-1}. Whilst, the far-field propagation is under influenced by remote resonance effects from the fast-travelling Lamb wave pulses in the layered atmosphere, resulting in a global, meteo-tsunami propagating over great distances at the speed of approximately 310 ms^{-1} or 1,100 kmh^{-1}, much higher than that of conventional tsunamis. In the 2022 HTHH case, the early arrivals of relatively small-amplitude leading ocean waves (soon after called the meteo-tsunami) before the conventional tsunami revealed the air-sea dynamic coupling that produced unusually global, trans-oceanic tsunamis. Thus, in this case Eq. (4.14) is no longer applied just because $t_{\text{obs}} < t_{\text{est}}$.

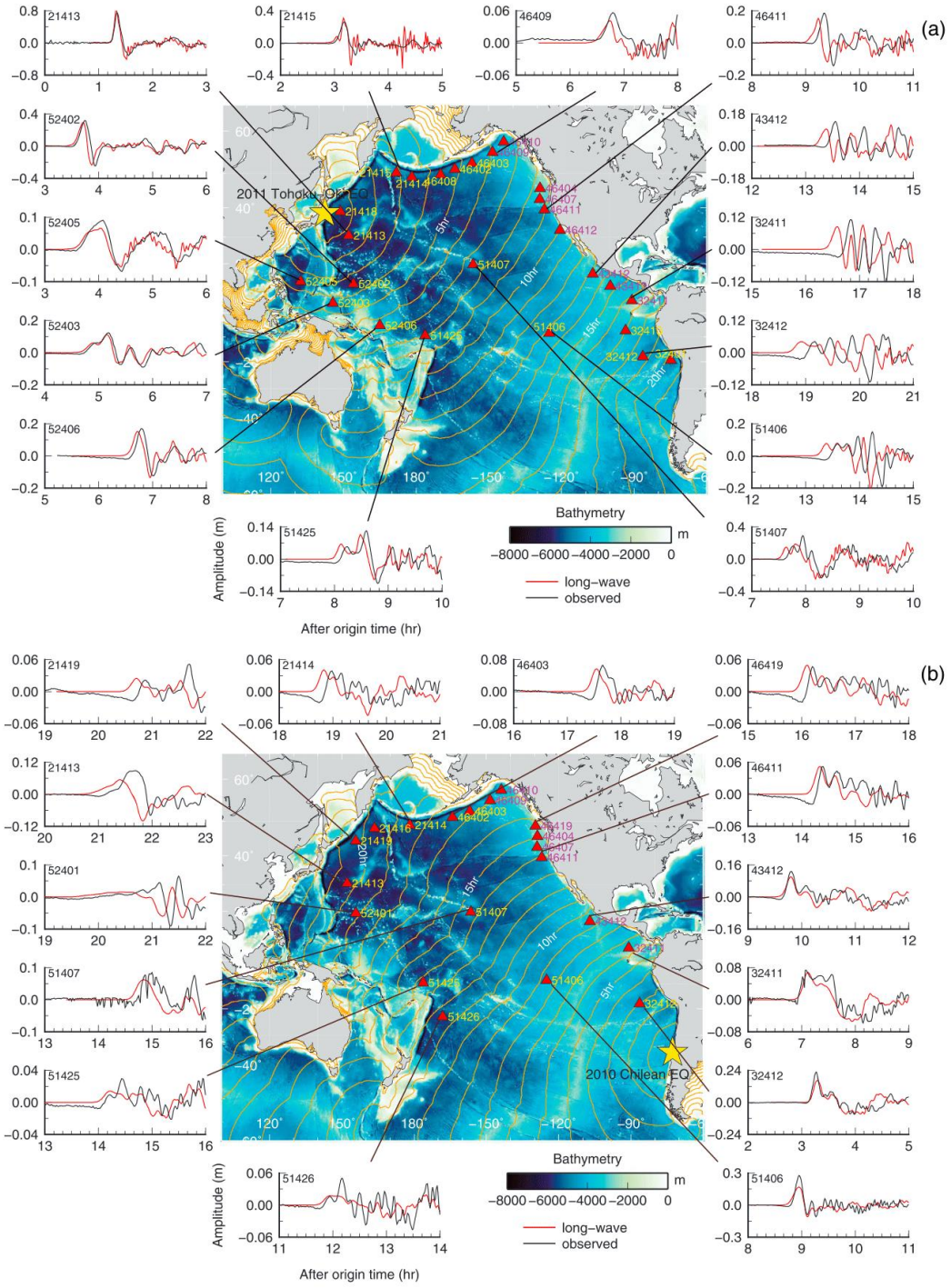

Figure 4.3. Comparisons of tsunami waveforms generated from long wave theory and observation for the 2011 Tohoku, Japan in (a) and the 2010 Maule, Chile events in (b). Yellow stars indicate the epicenters for both cases while red triangles show locations of DART buoys involved (taken from Watada et al., 2014).

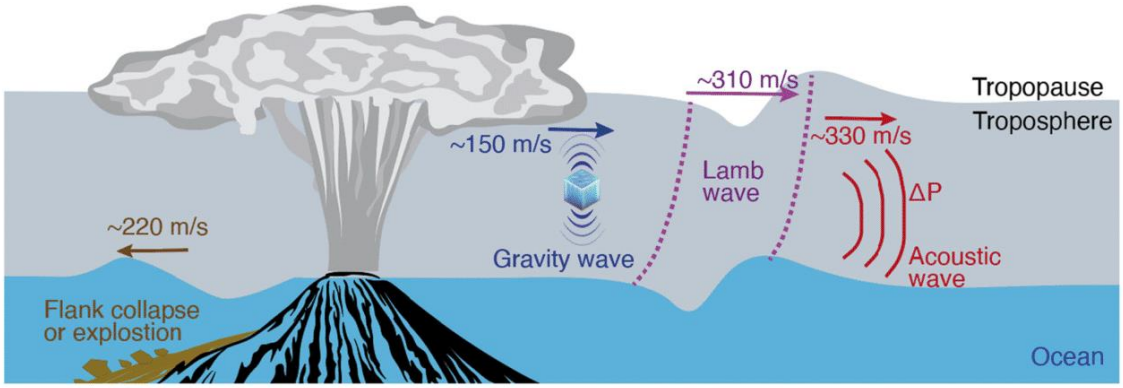

Figure 4.4. Sketch showing four tsunamigenic source mechanisms for the 2022 HTHH case (taken from Santellanes et al., 2022).

Here we provide below in Fig. 4.5 the results of numerical simulations on travel times calculated based on the shallow-water wave approximation for the conventional tsunami and the fast-travelling leading ocean waves owing to the coupled air-sea interaction for the meteo-tsunami derived for the 2022 HTHH case.

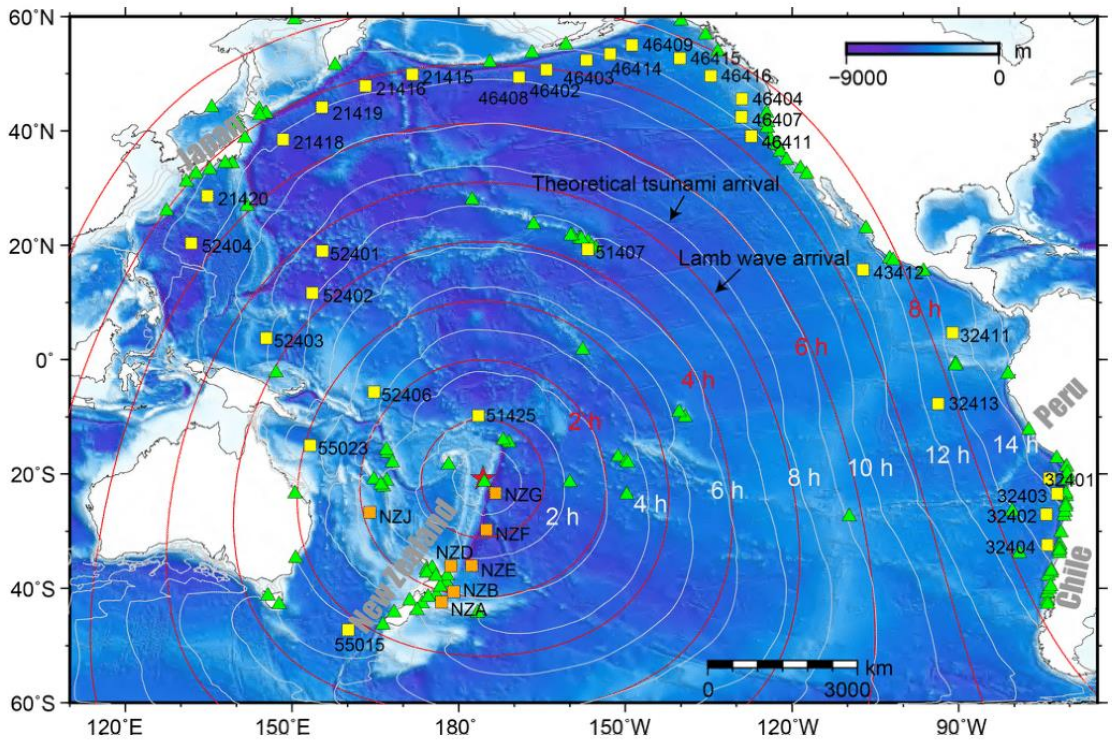

Figure 4.5. Sketch showing simulated travel times for the 2022 HTHH case where white contours represent estimated travel times based on conventional tsunami propagation and red contours denote observed travel times based on Lamb wave speed (taken from Hu et al., 2023).

4.5 Exercises

Answer clearly to the following questions regarding the content of Chapter Four.

1. Why are corrections to the speed formulation for tsunami propagation important ?
2. What are possible sources of factors affecting the speed of a propagating tsunami ?
3. Describe clearly factors slowing or speeding a tsunami (resulting in a reduced speed or an increased speed, respectively) during its propagation in the open ocean.
4. Given that the horizontal components of the momentum and continuity equations, respectively, as follows

$$\frac{\partial}{\partial t}(d+\eta)\,u = -g(d+\eta)\frac{\partial \eta}{\partial x} \tag{4.14}$$

$$\frac{\partial}{\partial t}d + \frac{\partial}{\partial x}(d+\eta)\,u = 0 \tag{4.15}$$

   where x represent the axis along which a tsunami wave propagates; other symbols have the same meaning as before in the text. Obtain the speed of a tsunami based on the shallow-water wave approximation that is frequently called the long wave speed.
5. What makes different between the 2022 Hunga Tonga-Hunga Ha'apai tsunami case and conventional tsunamis induced by earthquakes of seismic origin ?

Chapter Five

ENERGY AND AMPLITUDE MEASUREMENTS

This chapter examines characteristics of tsunami propagation from the source region to numerous tsunami monitoring stations at varying coastal locations in terms of energy and amplitude measurements. While the dispersive effects may reduce tsunami speed resulting in delayed arrivals or conversely atmospheric disturbances may be speeding up the wave ending up with early arrivals for the leading front (as earlier explained in §4.4), it has not yet been further discussed what happens to the energy and amplitude during the propagation. In this context, the decay or *e*-folding time of the energy (here measured using tsunami maximum amplitude attenuation with travel distance and/or travel time) within ocean basin is of fundamental importance for tsunami alert in various locations around the globe. Equally important and factual to coastal communities in developing countries, a lack of knowledge of time evolution of tsunami wave height or amplitude during the propagation from offshore to onshore is a long problem in tsunami research. When arriving at shorelines, extremely increased maximum amplitudes due to shoaling and wave effects cause severe fatalities, building damage and infrastructure destruction. This problem has been an important issue within the context of disaster risk reduction as it gives rise to the significance of run-up and inundation estimates at the first place. These issues will be explained in details in the following sections.

5.1 Energy and Amplitude Attenuation

The need for a better understanding of tsunami energy and amplitude attenuation with respect to travel time and distance from a tsunami source to a particular location is crucial for the development of a reliable tsunami early warning and hazard analysis. Estimate of onshore tsunami wave heights or run-ups requires accurate calculation of changes in tsunami maximum amplitude during the propagation. Careful examination of observed tsunami waveforms for the 2022 HTHH tsunami case freely accessible at https://www.ngdc.noaa.gov/hazard/dart/2022tonga.html has shown a unique decrease in the maximum amplitude with increasing epicentral distance. Energy attenuation can be examined using both spatial and temporal variations of the maximum amplitude during the propagation. As with the time measurements, the amplitude variations are

accounted for two regimes of observations. The observed amplitude drops rapidly during the initial stage of tsunami excitation in the near-fields before entering the second stage, where the wave advances with almost constant amplitude in the far-field measurements. Below are graphs showing how the amplitude evolves with travel distance (Fig. 5.1) and estimated travel time (Fig. 5.2) in different manners.

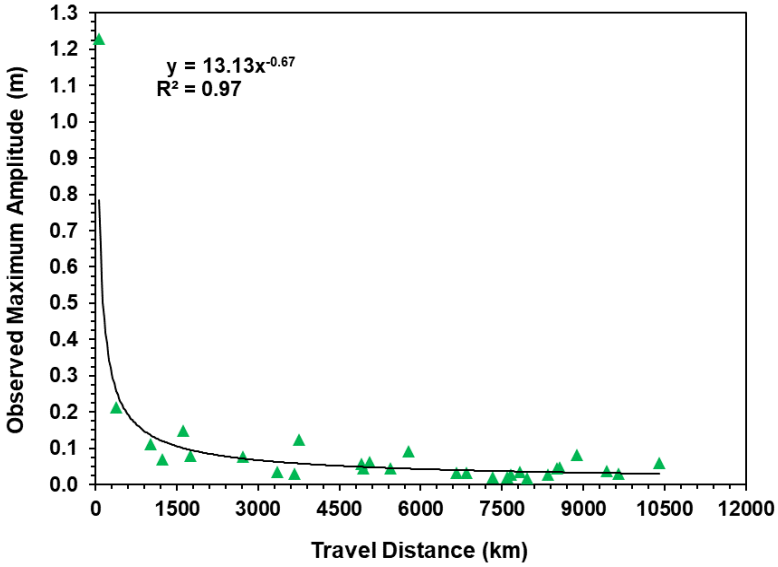

Figure 5.1. The observed amplitude against travel distance for the 2022 HTHH tsunami (taken from Realita et al. 2024).

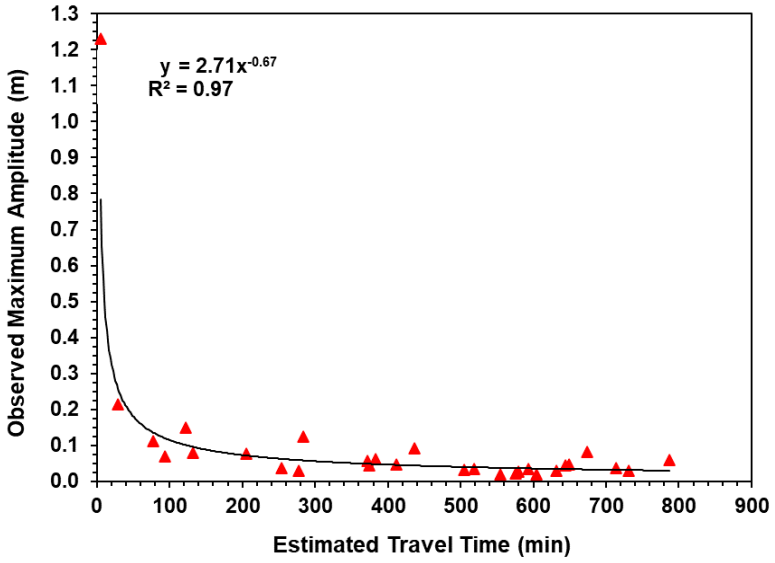

Figure 5.2. The observed amplitude against travel time for the 2022 HTHH tsunami (taken from Realita et al. 2024).

There seems two different ways of determining the HTHH energy decay (*e*-folding) time. The first one is likely to be approximated by travel time taken by a conventional tsunami propagating at the long wave speed from the volcano to a DART station numbered 32401, located offshore the northern Chile with water depth of 4,830 m (the farthest station). As wave energy dissipation through ocean processes during the propagation includes wave energy absorption by continental shelves and the propagation distance, the HTHH energy radiation and corresponding amplitude are then much attenuated when the wave arrives at coastal regions in Chile, far away from the volcano. Using the last red triangle seen in Fig. 5.2, we estimate the energy decay (*e*-folding) time to be about 790 minutes, which is about 13.2 hours from the onset time (Realita et al., 2024), close to 14 hours depicted by the white contour in Fig.4.5.

However, when a meteo-tsunami is present in distant observations for the HTHH case the above estimate seems wrong. We recalculate the HTHH decay time by looking over the data provided by DART 32401. It can also be predicted using 790 minutes divided by a factor of 1.38 (an empirical ratio of the observed meteo-tsunami to the long wave speed, see in Realita et al., 2024), which is 572.5 minutes ≈ 9.5 hours, in good agreement with 10 hours taken to be the simulated travel time of the meteo-tsunami from the volcano to DART 32401, as depicted by the red contour in Fig. 4.5.

Tsunami hazard analysis and associated risk of the 2022 HTHH case is of significance to the existing Indonesian tsunami early warning system (Ina-TEWS) as it is designed for detection of tsunami generation induced by tectonic earthquakes only. The recent 2018 Sunda Strait tsunami is triggered by complex volcanic processes (see §2.3 or alternatively Fig. 2.5). Hence, for Indonesia the implication of the 2022 HTHH tsunami analysis and associated risk may help better preparedness in response to future tsunami potential induced by seismo-tectonic sources or volcanic processes, including the one driven by atmospheric forcings.

In order to complete information about the behaviour of tsunami energy and amplitude attenuation for trans-oceanic tsunamis, we provide self-similar graphs developed from seven trans-oceanic tsunamis across the Pacific. The graphs illustrated in Fig. 5.3 are formed using normalised quantities in maximum amplitude and travel time. It is obvious from Fig. 5.3 that the maximum amplitude for the seven tsunami cases considered likely behaves in the same manner with respect to travel time. The observed amplitude changes in different rates in which much attenuation occurs in the near-field, compared with that in the far-field.

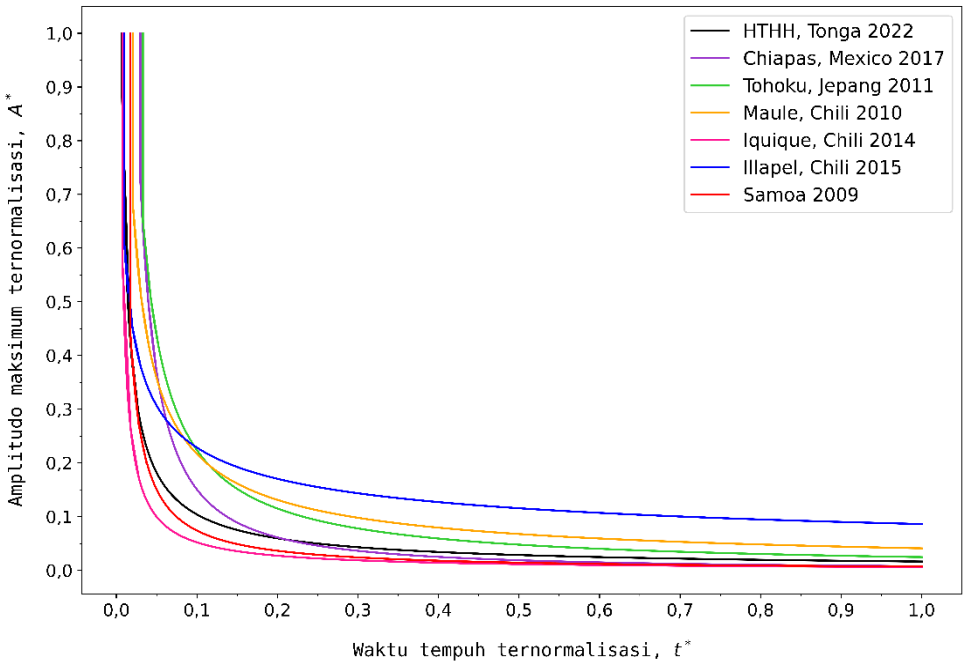

Figure 5.3. The normalised amplitude as a fitted power function of the normalised travel time for seven trans-Pacific tsunamis (taken from Chapter 4, Final Project by Dwi Maulidia, 2023).

5.2 Tsunami Wave Height Evolution

When a tsunami wave approaches coastal lines, bottom topography and its bathymetry affect the wave in a way that wave effects, such as refraction, diffraction, reflection and shoaling phenomena could possibly cause focusing or defocusing of tsunami energy, or equally alternative, changes in tsunami wave height. Therefore, tsunami dynamics and its behaviour in the coasts in terms of tsunami wave height or amplitude evolution are important to examine. Different from surface wind-waves, where these waves 'break into pieces' when the wave heights reach a certain value at a surfing zone, however, owing to its extreme length a tsunami behaves differently when arriving at shorelines.

Two kinds of 'change in waveform' of propagating tsunamis have been identified based on field observations. The first kind is a situation in which a gradual rise of ocean water and fall of ocean water occur with no water wave breaking (involving large turbulence, air entrainment and energy dissipation), as observed in tsunami arrivals at coasts with steep continental shelves and/or slopes. The second one occurs when tsunamis arrive at beaches with milder sloping topography, hence the waves break at offshore locations resulting in the formation of leading fronts called bores. Another phenomenon could also

be seen from onshore observations but not discussed here. For any waveform change, once the tsunamis reach the coasts, an amount of part of the energy is reflected and dissipated but a major one would inundate coastal areas, creating a serious problem for coastal communities.

Figure 5.4 provides the definitions of terminologies used in tsunami inundation process. The inundation area corresponds to tsunami horizontal penetration inland; it is bounded by the shoreline and the inundation line. Tsunami run-up is one of the most important quantities in a zone of mitigation (see again §1.3), defined as the height of the farthest point of horizontal inundation distance inland measured from the mean surface level. While inundation height is the difference between the sea surface and the mean sea level at the time of inundation, subsequently, it changes along the inundation area. Moreover, the run-up does not always coincide with the maximum inundation height, as shown by top and bottom panels of Fig. 5.4.

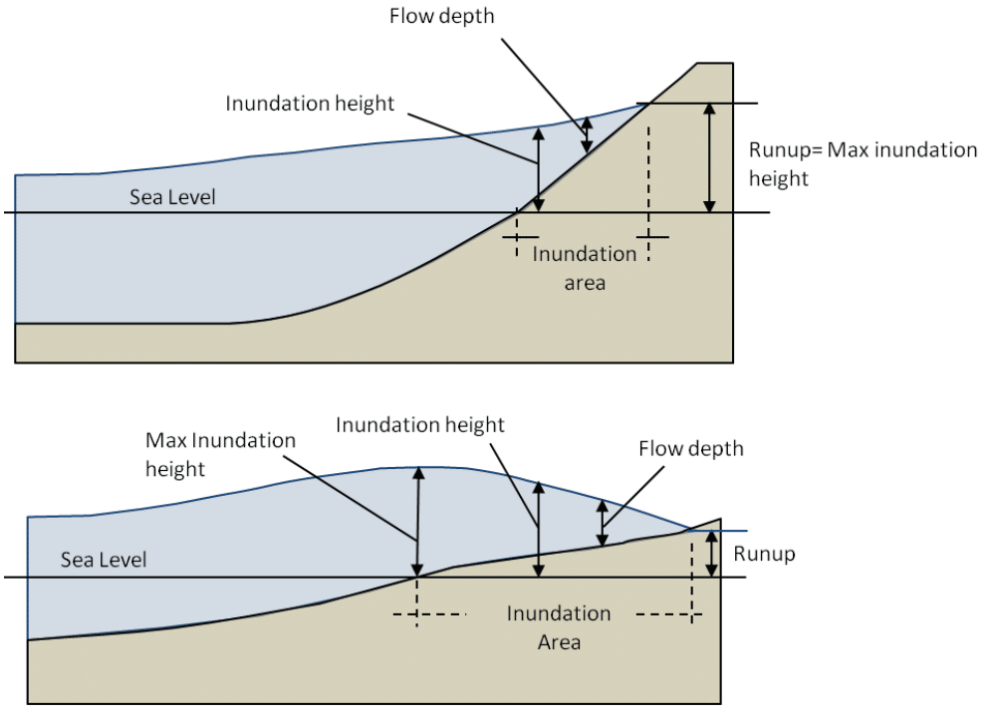

Figure 5.4. Definitions of tsunami run-up and inundation for two beaches with (a) a steep slope and (b) a mild slope (taken from Analysis of Tsunami Propagation in Coastal Areas: Lessons from Past Tsunamis by R. Aránguiz, 2014).

The flow depth is defined as the difference between the ground-base surface elevation and the seawater surface during inundation. It also changes along the inundation area.

This quantity is important in determining tsunami impact on damaged properties and infrastructures. During the inundation process, tsunamis can cause several impacts on coastal areas, such as severe erosion or sand sedimentation along the shorelines, as indicated by several photos taken after the 2009 Samoa tsunami in Fig. 5.5.

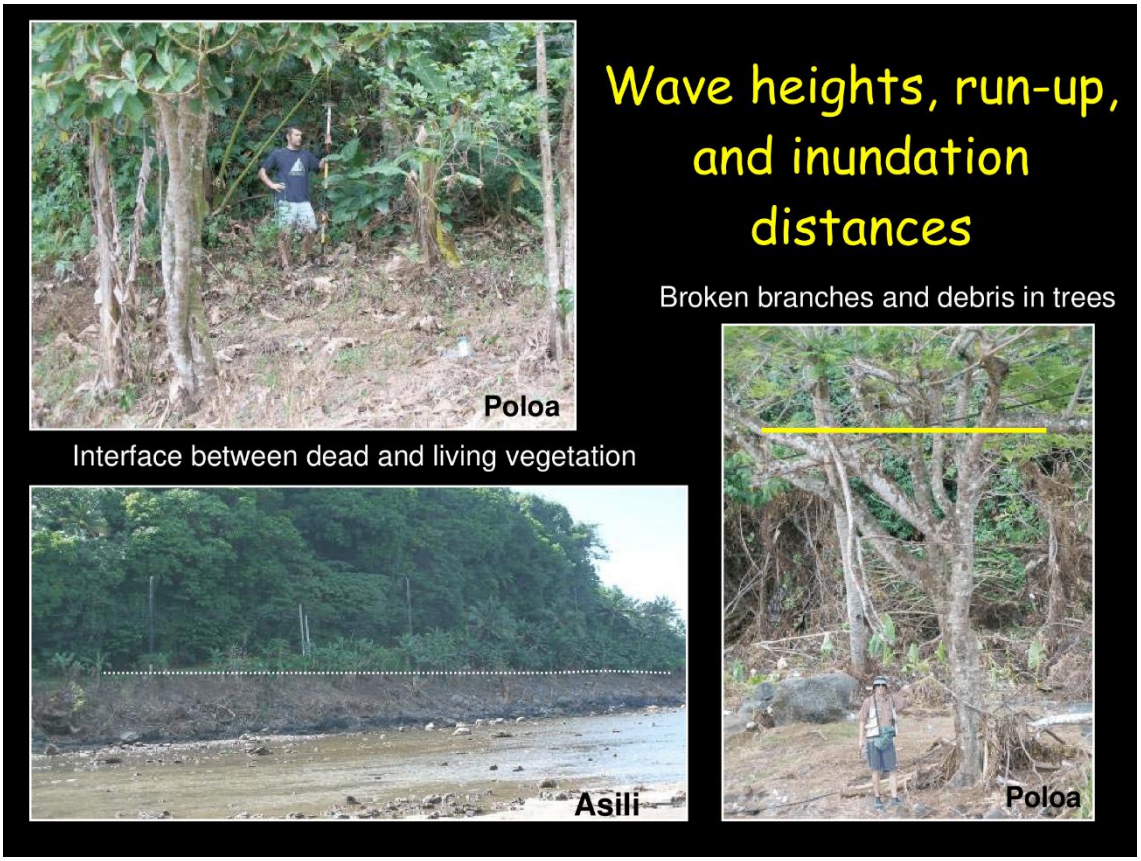

Figure 5.5. Post-tsunami surveys after the powerful 29 September 2009 Samoa tsunami strike, showing water levels as tsunami parameters in Poloa and Asili in the western coasts of Samoa, where run-ups were found to be 11 m in both villages and horizontal inundations were measured to be 70 m in Poloa and 185 m in Asili (taken from The Samoa Tsunami of September 29, 2009: Preliminary Field Data on Tsunami Inundation in American Samoa by Gelfenbaum et al., 2009).

It is now time to derive the energy transferred during tsunami propagation that involves the change in wave height or maximum amplitude. We begin with physical grounds on the problem in question, where transfer of energy does not account for energy dissipation owing to bottom friction, wave dispersion and viscous effects. With the total energy of travelling tsunamis remains constant, the kinetic energy is reduced (along with reduction in speed) as the water depth decreases and subsequently, the potential energy increases

in such a way that the total energy is equally distributed to both the kinetic and potential energies (detailed derivation is left for the reader). Thus, for the waveform illustrated in Fig. 3.4, the total energy per unit area ε is related to the wave height H by

$$\varepsilon = \frac{1}{8}\,\rho g H^2 = \frac{1}{2}\,\rho g a^2 \tag{5.1}$$

where $H = 2a$ has been used for a representing the maximum amplitude and ρ denotes the mean density. Equation (5.1) holds for the shallow-water wave approximation and serves as an ingredient for tsunami run-up estimates by both the basic Green's law and the extended Green's law that will be discussed in the following sub-sections. In addition, the proportionality of $\varepsilon \propto a^2$ is relevant to classical physics.

5.2.1 Run-Up Estimate by Basic Green's Law

The first step to do towards realising tsunami forecasting based on offshore monitoring of tsunami passage is to determine the basic relationship between tsunami wave height or maximum amplitude observed at offshore observatories and that measured from coastal observatories. The monitoring instrument used could potentially be DART buoys and coastal tide gauges or even ocean bottom pressure gauges. In the measurements, nearshore wave conditions are therefore critical to prediction of tsunami wave height or maximum amplitude when the wave arrives at shorelines. A physical quantity of interest under investigation is a possible run-up, being estimated to reduce property losses and fatalities for people at risk. In turn, post-event field surveys performed normally confirm that run-up data distribution is indicative of tsunami impact on affected coastal regions.

We begin derivation of run-up estimate with calling the energy per unit area ε in Eq. (5.1) as the energy density. The rate at which the energy density is displaced from a point at an offshore location to a point at a particular onshore station is termed flux of energy ϕ, mathematically defined to be the product of tsunami long wave speed given by Eq. (3.39) and the energy density. Thus, the energy flux is written as

$$\phi = \sqrt{gd}\;\frac{1}{2}\rho g a^2 \tag{5.2}$$

Theoretically, the flux of energy remains constant (for which it is called conservation of energy flux) during propagation from offshore locations to onshore stations. Hence,

$$\frac{d\phi}{dx} = \frac{d}{dx} d^{1/2} a^2 = 0 \tag{5.3}$$

Equation (5.3) follows that the flux of energy is conserved during the wave motion along the propagation axis x and thus we can write

$$d_1^{1/2} a_1^2 = d_2^{1/2} a_2^2 \tag{5.4}$$

where indices 1 and 2 on the left and right sides are offshore and onshore measurements, respectively. Equation (5.4) shows evolution of the wave height or maximum amplitude when the wave 'feels' a change in water depth (shoaling effect) during propagation. Then, it is free to write $d_1 = D$ and $d_2 = d$ as well as $a_1 = \eta$ dan $a_2 = R$, yielding

$$R = \left(\frac{D}{d}\right)^{1/4} \eta \tag{5.5}$$

where D and d are the offshore and onshore local depths, respectively, η is the maximum amplitude recorded by an offshore observatory and R is run-up estimate due to the effect of shoaling. The shoaling effect appears to be influenced by the difference in water depth between offshore locations and onshore stations.

Equation (5.5) is frequently called the basic Green's law, confirming that a tsunami wave may pass unnoticed out at sea (due to relatively small amplitude in the open ocean) but growing much higher as it approaches a coast. The basic Green's shoaling law with only external parameters of water depth included for prediction of tsunami run-up height seems to oversimplifying factors originating from shoreward tsunami wave propagation that may influence on the run-up. The Green's shoaling prediction, however, can be used to the first order to estimate the run-up with caution in the sense that the non-linearity of the governing equations describing the dynamics of a tsunami as it approaches a beach and corresponding complexities, such as local bathymetry and coastal topography are not yet included in the prediction.

5.2.2 Run-Up Estimate by Extended Green's Law

Run-up estimate should not underestimate possible factors that may play a key role in the prediction. Refraction effect, the one among these factors, is found to be the cause for the deviation of run-up measurements from the basic Green's shoaling law given in Eq. (5.5). The direction of propagation of a tsunami wave changes with spatial variation of the water depth. Such a change in the propagation direction is referred to as refraction, which follows Snell's law in classical optics. According to this law, both the angles of wave incidence and refraction relate to wave speeds at two regions of distinct depths. Because the wave speed is a function of water depth, as seen in Eq. (3.39), then the wave refraction comes in effect whenever there is a change in the depth. The angle of refraction becomes smaller, along with the speed reduction, as the depth decreases. Illustrated in Fig. 5.6, the onshore propagation of a tsunami wave near a cape and a bay at once.

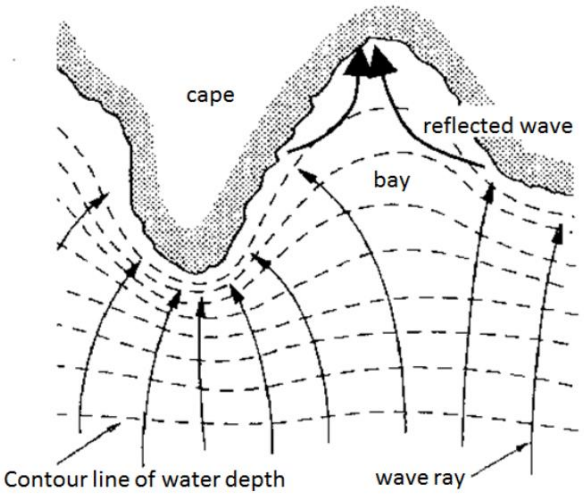

Figure 5.6. The incident energy of a tsunami wave near the tip of a cape is concentrated owing to refraction following the change in water depth, which enables the wave amplitude to grow higher. In a bay or an inlet, tsunami wave height can also increase owing to the effect of reflection and because of the amplification effect owing to a decrease in the width of a wave ray interval (taken from Tsunami Basics for Engineering by SATREPS Chile Tsunami Project Publication Series Volume 3, 2016).

To take the effects of both the changes in the water depth and the wave ray interval width, we provide a sketch in Fig. 5.7, showing the propagating tsunami wave, which encounters two effects at once, that is, the shoaling (external factor) as it comes from ocean basin and the wave ray interval (internal factor) as it comes from wave behaviour. Using this, run-up estimate with the inclusion of the wave ray interval width is ready to do.

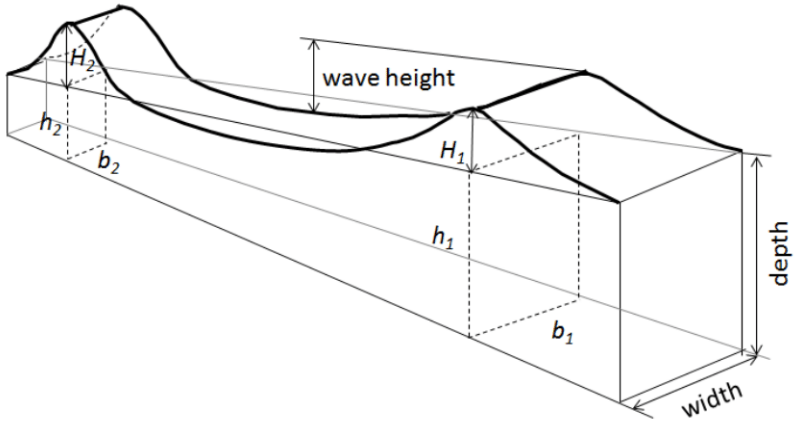

Figure 5.7. The increased wave height owing to changes in the water depth and/or the wave ray interval width (taken from Tsunami Basics for Engineering by SATREPS Chile Tsunami Project Publication Series Volume 3, 2016).

Although Eq. (5.5) can be used to estimate run-ups in beaches with shallow depths under the shoaling effect, it has not yet taken the effects of coastal morphology and geometry into account. Tsunami wave height or maximum amplitude variation is also influenced by wave behaviour, such as reflection and refraction. While reflection is only effective to affect the propagation when the wave meets islands or volcanic barriers on its way to coastal regions or multiple reflection within a semi enclosed ocean basin, such as a bay or a harbor, wave refraction is more effective to do so than the reflection is. In particular, when a tsunami approaches a cape and a bay, as shown in Fig. 5.6, the width of the ray interval changes, narrower near the tip of the cape or near the inlet of the bay.

Regarding mechanism of transfer of energy, tsunami energy is radiated by the wave from the source to varying locations in cylindrical symmetry. With no losses of the total energy or alternatively the energy density ε remains constant, Eq. (5.1) becomes

$$\epsilon = \frac{1}{2}\,\rho g a^2 L = \frac{1}{2}\,\rho g a^2\, 2\pi b \tag{5.6}$$

where ϵ is the total energy per unit length and $L = 2\pi b$ is the characteristics length of water column having cylindrical surface with b denotes the geometrical-spacing width, the distance between two adjacent wave fronts or the width of the wave ray interval. Then, the rate at which the total energy per unit length ϵ is displaced from one place to another in the ocean is written as ψ. This quantity is more relevant to accommodate both shoaling and refraction effects on run-up estimate. Mathematically, ψ is written as

$$\psi = \sqrt{gd}\;\rho g a^2\,\pi b \tag{5.7}$$

With the help of Eq. (5.7), then Eq. (5.3) changes into

$$\frac{d\psi}{dx} = \frac{d}{dx} d^{1/2} a^2 b = 0 \tag{5.8}$$

Repeating the physical meaning of the indices 1 and 2 for Eq. (5.8), we have energy flux conservation in the form of

$$d_1^{1/2} a_1^2\, b_1 = d_2^{1/2} a_2^2\, b_2 \tag{5.9}$$

where b_1 and b_2 are the distances between two adjacent wave fronts or the wave ray interval widths at offshore and onshore locations, respectively. When the same treatment as before is applied to all symbols in Eq. (5.9), that is, $d_1 = D$, $d_2 = d$, $a_1 = \eta$, $a_2 = \mathcal{R}$, $b_1 = B$ and $b_2 = b$, then Eq. (5.9) becomes

$$\mathcal{R} = \left(\frac{D}{d}\right)^{1/4} \left(\frac{B}{b}\right)^{1/2} \eta \tag{5.10}$$

where $\mathcal{R}$ is run-up estimate with the inclusion of refraction effect.

In areas with a smooth bathymetry and a bottom topography, tsunami run-ups with shoaling and refraction effects $\mathcal{R}$ based on the wave ray separation generally presents no problem. However, in the case of an irregular bathymetry, the pattern of wave rays may become chaotic. In such a case, a direct transformation of wave ray separation into local wave heights, if possible, yields highly erratic estimates of run-up. Frequently occurred, adjacent wave rays or wave fronts will cross and fundamental problems may then arise. In this case, the wave ray separation becomes zero and the corresponding wave height or maximum amplitude would be infinite, as diffraction effects are ignored.

5.3 Tsunami Inundation

As earlier mentioned in §1.3 and then graphically illustrated in Fig. 5.4, it is obvious that tsunami inundation is the horizontal, inland penetration of the waves from the shoreline. Inundation distances vary greatly along the shorelines, depending on influencing factors that include the source strength, tsunami intensity, coastal topography and morphology, nearshore bathymetry, bottom roughness, coastal vegetation, land use and man-made structures. All these factors play a vital role in constraining the inundation limit, which is frequently determined by measuring the distance over which destroyed vegetation and scattered tsunami debris are found inland as well as eyewitness accounts of the incident. The inundation can also be estimated by paleo-deposit distribution from past tsunamis. Knowledge of paleo-tsunami parameters, for example, inundation and run-up is critical for well-designed town planning and disaster prevention along coastal regions.

Instead of only post-event field surveys, future observations in the aftermath of the event may use aerial and/or satellite imagery because the maximum inundation area might be underestimated as it is difficult to identify during the field surveys. This is just because measured run-up and inundation change with time. Different from run-up height, which is relatively easy to observe, inundation is difficult to measure. While run-up is estimated using either Eq. (5.5) or Eq. (5.10) derived from conservation of the energy density per unit area for the shoaling effect only or unit length for the inclusion of refraction effect, inundation distance limit seems only to be determined from post-event field surveys. This is why publications concerning with tsunami impact did not complete the report with prediction of inundation distance in addition to the results of the surveys. Instead, numerical modelling provides prediction of tsunami run-up heights for comparison.

Here we describe how tsunami inundation penetrates inland from the 2018 Palu Bay and the 2018 Sunda Strait tsunamis. To assess inundation, run-up, damaged buildings and

infrastructures in the 2018 Palu Bay event, field surveys were completed after the event. The results showed that the inundation is longer in the southern part of the bay owing to stronger multiple reflection around Palu City (bay resonance) and that also longer (with higher run-ups) in the western portion due to the traverse of Palu Koro fault line. Despite discrepancy in the causative source of tsunami generation in the 2018 Palu Bay tsunami, it was partly induced by earthquake-triggered submarine landslides, indicating how quickly the waves inundate coastal regions within the bay following nearshore landslides. There are unstable body structures at and near coastal areas (river mouths and reclaimed land using gravels and sands) in the western shore, where landslide-generated tsunamis could be observed from the videos made by eyewitness accounts. This shows the danger posed by unstable sediments at low-lying coastal areas, addressing the urgent need for site identification of possible land-slides to occur and adequate public information about local vulnerability to such a disaster in order to reduce disaster risk in the future.

Similar to the 2018 Palu Bay event, to a better look at the 2018 Sunda Strait tsunami, field surveys were conducted. The surveys include measurements of run-ups, inundation distances and tsunami propagation directivity, as shown in Fig. 5.8.

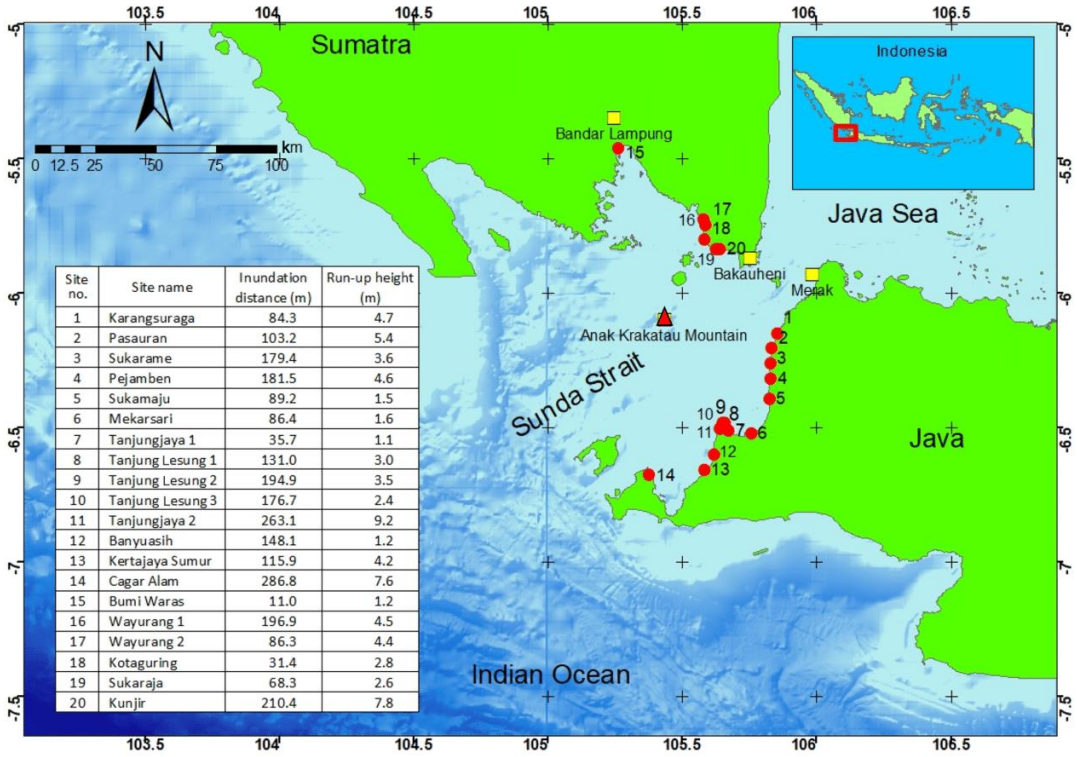

Site no.	Site name	Inundation distance (m)	Run-up height (m)
1	Karangsuraga	84.3	4.7
2	Pasauran	103.2	5.4
3	Sukarame	179.4	3.6
4	Pejamben	181.5	4.6
5	Sukamaju	89.2	1.5
6	Mekarsari	86.4	1.6
7	Tanjungjaya 1	35.7	1.1
8	Tanjung Lesung 1	131.0	3.0
9	Tanjung Lesung 2	194.9	3.5
10	Tanjung Lesung 3	176.7	2.4
11	Tanjungjaya 2	263.1	9.2
12	Banyuasih	148.1	1.2
13	Kertajaya Sumur	115.9	4.2
14	Cagar Alam	286.8	7.6
15	Bumi Waras	11.0	1.2
16	Wayurang 1	196.9	4.5
17	Wayurang 2	86.3	4.4
18	Kotaguring	31.4	2.8
19	Sukaraja	68.3	2.6
20	Kunjir	210.4	7.8

Figure 5.8. Data for inundation distances and run-up heights for each site of the field surveys performed in the aftermath of the 2018 Sunda Strait tsunami (taken from Widiyanto et al., 2020).

Although the method was apparently subjective as tsunami deposits are discontinuous and scattered over a flooded area, for example, sand sheets deposited on land vary greatly owing to the influence of sedimentary sources and local topography, the results were very promising to describe what was happening at the time the waves striking coastal regions in the southern Lampung and the western Banten Provinces.

5.4 Exercises

Answer clearly to the following questions regarding the content of Chapter Five.

1. Why are measurements of tsunami energy and amplitude so important ?
2. Figures 5.1 and 5.2 both are able to explain the behaviour of the observed amplitudes at distant observations but fail to explain the presence of a meteo-tsunami in the case of 2022 HTHH volcanic eruption and resulting tsunamis. Please, argue in favour of the meteo-tsunami travelling at a higher speed than conventional tsunamis.
3. Why are measurements of tsunami wave height evolution so important in the context of tsunami mitigation study ?
4. What basic physics principles are lying on the formulation of run-up estimates written in Eqs. (5.5) and (5.10) ?
5. Tsunami run-up heights measured along coastal regions within Palu Bay are found unexpectedly high from scattered tsunami traces during field surveys. What possible causes for the results of the measurements ?

This page is intentionally left blank

Chapter Six

TSUNAMI DISASTER MITIGATION

The 26 December 2004 Indian Ocean tsunami is considered one of the greatest tsunamis in modern times, where global media widely broadcasted its impact around the world. The reasons of the huge loss include the absence of tsunami monitoring instruments off the west-coasts of Sumatera Island and extremely limited awareness and preparedness of the government and local community. In response to the high number of casualties as well as property losses associated with the 'boxing day' tsunami, many countries having coastal inhabitants prone to tsunamis have developed tsunami early warning systems and mitigation plans. In the long term, if the growing awareness and preparedness for tsunamis in the future are maintained and the capacity building in society is developed, the well-prepared communities in both individual and institutional levels could reduce tsunami risk in terms of a decrease in the huge number of fatalities and financial losses. This requires willingness and significant investments in education from the government and any party for those living nearby coastal settlements vulnerable to tsunami potential, and school students (from primary to secondary level) and university students.

The 'now and then' existence of tsunami hazard awareness and preparedness in a country can be reflected by a number of factors, depending on whether the focus is placed on private citizens (the public or students) or institutional bodies (authorities or agencies). The level of awareness of local communities to tsunamis can be learned from analysis of their willingness to evacuate during recent events after the 2004 Indian Ocean tsunami. At the institutional level, there is a major concern hence corresponding political will to increase disaster preparedness through community relocation away from danger zones and to improve a tsunami alert system. This chapter discusses how tsunami awareness and preparedness in Indonesia at the citizen and institutional levels have increased since the 2004 Indian Ocean tsunami.

6.1 Vulnerability to Tsunami Hazard

Indonesia is considered one of the most active seismo-tectonic regions on Earth due to its unique position at the triple junction of the world major tectonic plates, completed with coastal lines of over 99, 000 km long. This tectonic setting makes not only Indonesia

as a country with the second longest of coastal lines in the world but also vulnerable to tsunami hazard. With an ever-increasing growth of Indonesian population, it is therefore important to consider tsunami risk in densely populated settlements nearby the coasts. The vulnerability of coastal inhabitants in Indonesia to a tsunami was clearly indicated by the global impact of the 2004 boxing day tsunami, which killed over 250,000 people along the west-coast of northern Sumatra and destroyed ecosystems, such as coral reefs, coastal forests and vegetation, sand dunes, and animal and plant biodiversity.

During post-tsunami field surveys, it is common to assess building damage in order to measure tsunami impact. Building damage and associated vulnerability assessment are important for future tsunami risk mitigation and evaluation through engineering design, casualties and financial loss estimates, and land use and emergency planning. It is then crucial to note that building vulnerability assessment forms only a stepped measurement in the overall risk evaluation (see Fig. 6.1).

TSUNAMI RISK = TSUNAMI HAZARD X **VULNERABILITY** X EXPOSURE

Tsunami hazard =	The probability of a potentially damaging tsunami occurring at a site within a given period of time.
Vulnerability =	The likelihood of losses (financial and casualty) given a tsunami of a particular intensity.
Exposure =	Quantification of the number of people and buildings at risk.

Figure 6.1. Three components of tsunami risk, where vulnerability is highlighted as it is the main application of building damage assessment (taken from Building Damage Assessment and Implications for Future Tsunami Fragility Estimation by Suppasri et al., 2015, Ch. 9 of Handbook of Coastal Disaster and Mitigation for Engineers and Planners, edited by Esteban et al., 2015).

Naturally, tsunami hazard cannot be reduced and even may potentially increase due to some reasons. Global exposure is increasing as a result of global trends, such as growing coastal populations due to rapid urbanisation of coastal cities and higher urban densities, causing people to settle for life in marginal locations at risk. Thus, it is clear from Fig. 6.1 that reducing vulnerability is the key element to reduce tsunami risk. While assessment of building damage and hence vulnerability relates probable losses to tsunami intensity, a more detailed assessment separates the assessment of likely building damage from estimated losses due to that damage. In this context, fragility is defined as the probability of building damage given a tsunami with a particular intensity whereas the loss model is defined as the probable human and financial losses for a given level of building damage. Further discussions on both tsunami fragility and loss model are not here provided.

6.2 Tsunami Mitigation Strategy

Generally speaking, tsunami risk along coastal settlements with dense population is high as this condition is prone to tsunami hazard. It is vital to consider tsunami mitigation strategies, which may take a variety of activities in these settlements. The key element to improve the resilience of coastal communities to tsunamis is a high degree of awareness and preparedness among the local population. It is possible to find a situation in which residents in the settlements may not have experience with previous tsunami occurrences. In this case, local wisdom in the form of, for example, mouth-to-mouth story-telling or indigenous knowledge of 'smong tradition' among the residents in Simeulue Island about past tsunamis has saved some residents in the 2004 Indian Ocean tsunami case.

However, to maintain the traditional knowledge where it is present needs to enhance people's awareness against future tsunamis through formal and non-formal education at all levels that are usually facilitated by Indonesian Agency for Meteorology, Climatology and Geophysics (BMKG), as illustrated in Fig. 6.2. This includes, for example, running childhood parenting, relevant public training, and frequent tsunami drills in schools and universities for both normal and disabled persons so that people know what to do exactly at the emergency times. Such drills appear effective in reducing the rates of fatalities and form the central part of efforts for disaster risk reduction.

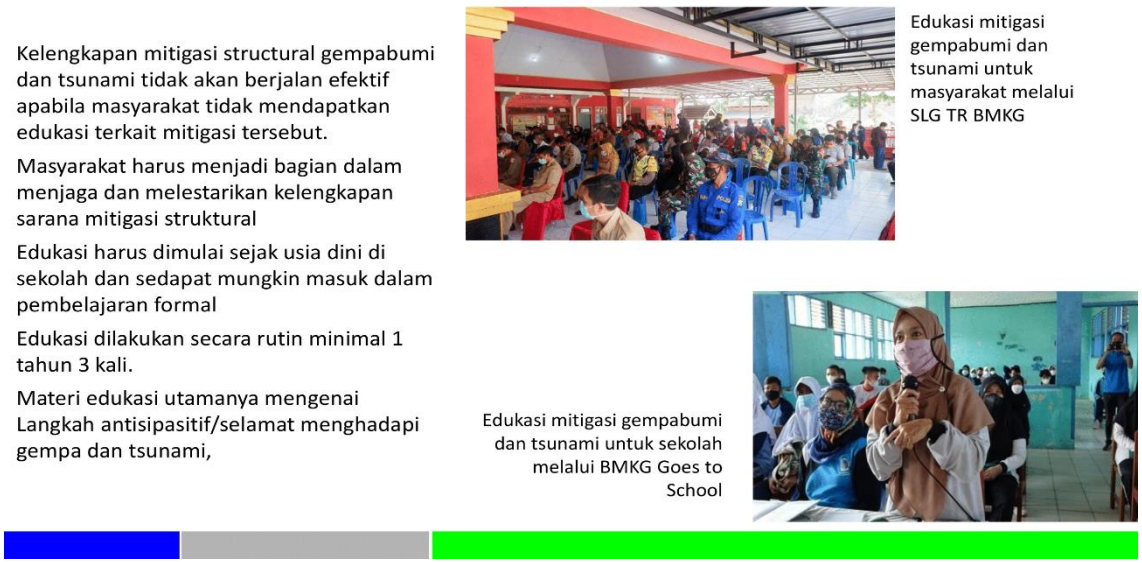

Figure 6.2. Routine jobs to do by BMKG, socialising earthquake and tsunami disaster education to both public and school communities (taken from Sadar dan Siaga Gempa Bumi dan Tsunami demi Mewujudkan Ketangguhan Daerah by Suci Dewi Amugerah, BMKG Pusat, a webinar series of disaster mitigation study on 16 March 2022).

An effective method of minimising tsunami risk is to develop tsunami early warning with a quick and accurate good working system to minimise any insufficient or false warning, as shown in Fig. 6.3. Such a system is equipped with offshore and onshore monitoring instruments for coastal communities vulnerable to tsunami hazard potential.

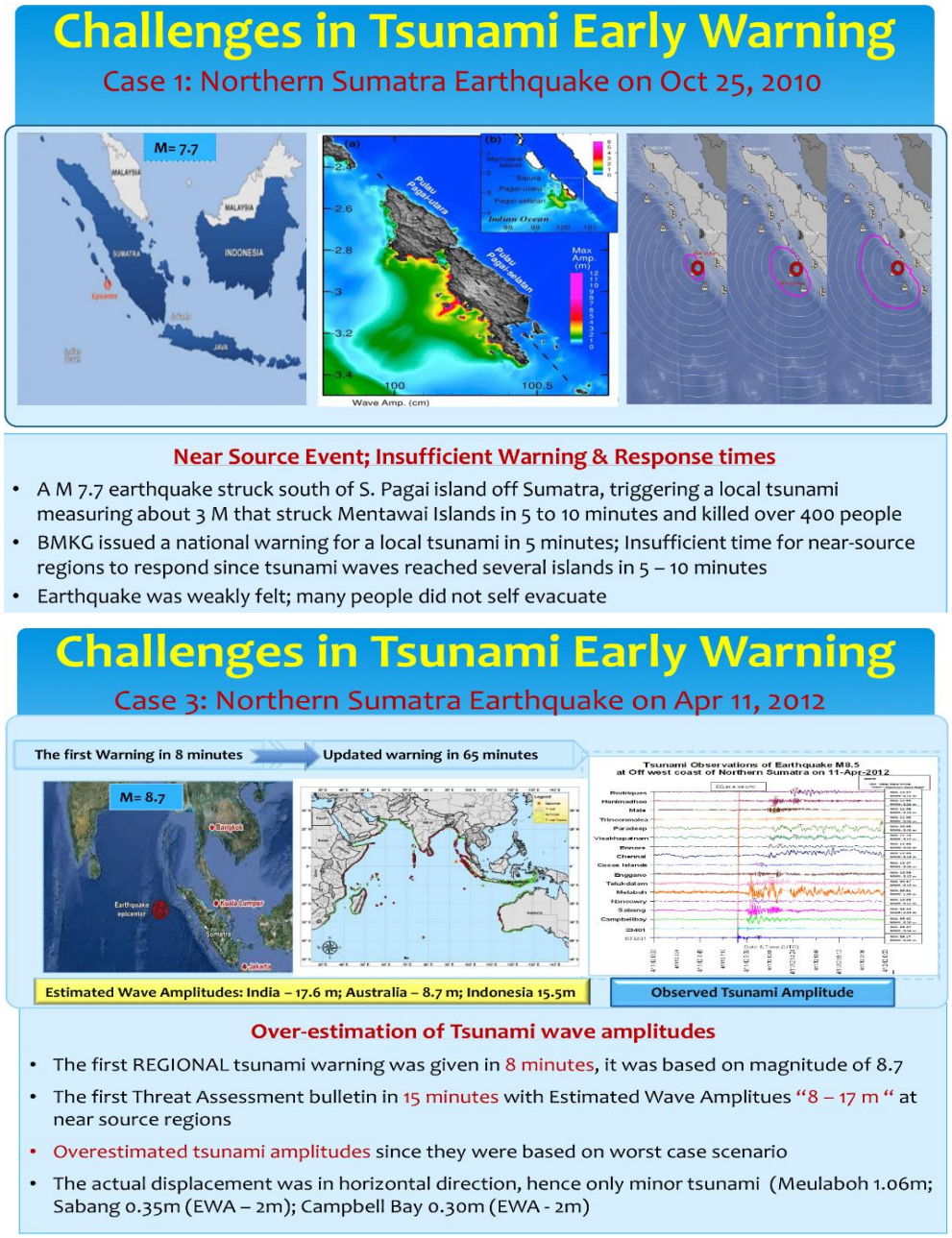

Figure 6.3. Examples of tsunami false warning issued for two events with the hypocentres located off the west-coast of Sumatera Island in 2010 (top panel) and 2012 (bottom panel) (taken from Tsunami Warning by T. Srinivasa Kumar, Indian Tsunami Early Warning Centre, 2016).

While a tsunami early warning system has long existed in the Pacific, the development of a similar system in the Indian Ocean came late as it is only available for use following the destructive 2004 Indian Ocean tsunami. The warning system should be accompanied with local evacuation maps and clearly marked routes and signs that allow residents of all ages and sexual gender with any physical condition to easily evacuate (see Fig. 6.4). This should include signs and maps of safe evacuation for external visitors from overseas usually coming to coastal areas for tourism, such as Parangtritis in Java, Kuta in Bali and Phuket in Thailand.

Figure 6.4. Best practices of community involvement of good awareness and preparedness in minimising tsunami risk by creating evacuation routes and signs (taken from Sadar dan Siaga Gempa Bumi dan Tsunami demi Mewujudkan Ketangguhan Daerah by Suci Dewi Amugerah, BMKG Pusat, a webinar series of disaster mitigation study on 16 March 2022).

Nevertheless, the most effective way to mitigate tsunami risk would be to relocate people with low-rise houses in low-lying coastal settlements to higher ground. But this does not appear to be realistic, either because there are no appropriate high-ground places nearby the residential area or local residents want to live near the coast for ease of daily fishing. In such a case, the residents could explore the possibility of building tsunami shelter or making easy evacuation routes to higher ground, where people are easily transported to safe locations within a short period of time.

For public needs, it seems that emergency status describing the level of tsunami alertness associated with a possible danger is of importance (see Fig. 6.5). Within a limited time before, during and after a tsunami strike, the emergency status may or may not change

depending upon a series of records of relevant parameters and corresponding analyses. Thus, the status may go up or down a level, for which simple but clear communication between the authorities and local society as well as the third party remains necessary. Such communication through media of any kind of modes (see Fig. 6.6) will be useful for action in response to the latest condition during and aftermath of a tsunami.

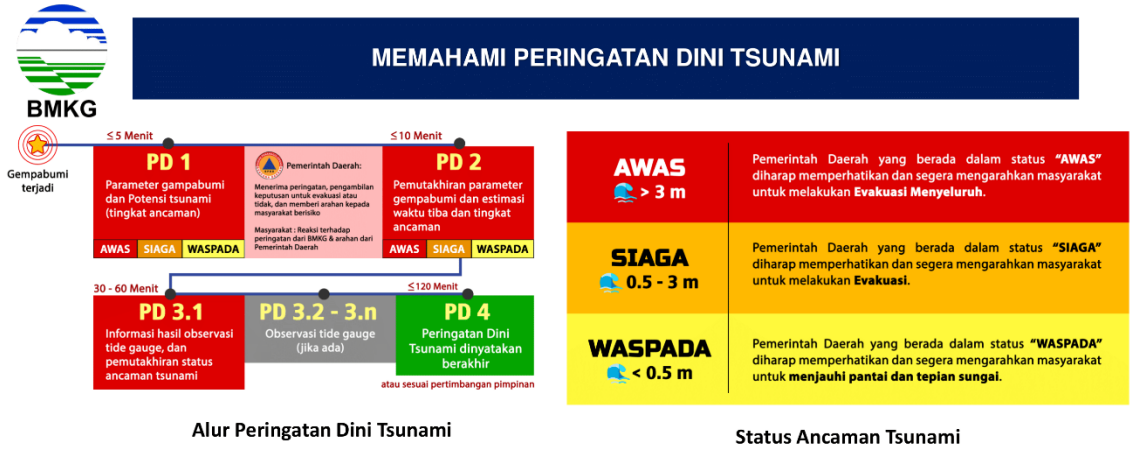

Figure 6.5. Gradually increasing levels of tsunami alertness from the lowest to the highest (taken from Membangun Budaya Kesiapsiagaan terhadap Bahaya Tsunami by Suci Dewi Amugerah, BMKG Pusat, a webinar series of disaster mitigation study on 28 May 2021).

Figure 6.6. Various modes of communication developed to disseminate tsunami alert (taken from Membangun Budaya Kesiapsiagaan terhadap Bahaya Tsunami by Suci Dewi Amugerah, BMKG Pusat, a webinar series of disaster mitigation study on 28 May 2021).

6.3 Roles of the Authorities and Agencies

Regional Disaster Management Agency (BPBD) is responsible for managing activities associated with disaster management at municipal and provincial levels. BPBD is known as part of National Agency for Disaster Countermeasure (BNPB) at a national institution. Before a disaster, the relevant agencies at all levels provide guidelines and direction for disaster management, prevention and preparedness. In this sense, effective strategy for disaster risk reduction (DRR) is organised and run along with reliable early warning and building community resilience. During a disaster, the relevant authorities and agencies both manage emergency tasks, including running quick response, updating status alert, evacuating to appropriate shelters, providing food and water supply and life equipment. In the aftermath of a disaster, the likely jobs to do are to include site rehabilitation, property reconstruction and inhabitant relocation. The description of these management tasks can be seen in Fig. 6.7 below.

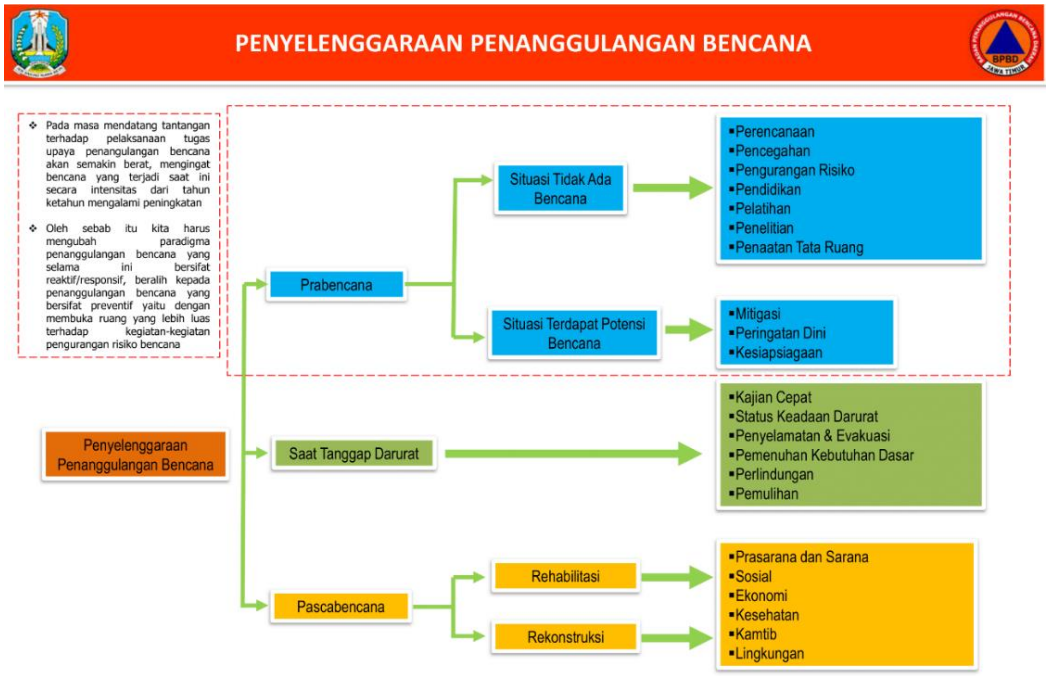

Figure 6.7. Various jobs to do in different stages by BPBD in response to emergency conditions due to a disaster (taken from Kesiapan Daerah dalam Pengurangan Risiko Bencana by Gatot Soebroto, BPBD Jawa Timur, a webinar series of disaster mitigation study on 28 May 2021).

Normally, regular board meeting as shown in Fig. 6.8 is held by the authorities and BPBD to discuss regional and national issues associated with types of disasters, where one of

the topics is tsunami potential in particular regions. The discussions may be based on probabilistic hazard analysis and its associated assessment.

Figure 6.8. On regular meeting by BPBD Jawa Timur, discussing the best strategy for managing disasters (taken from Kesiapan Daerah dalam Pengurangan Risiko Bencana by Gatot Soebroto, BPBD Jawa Timur, a webinar series of disaster mitigation study on 28 May 2021).

Due to its seismo-tectonic settings, many parts of Indonesian territory are vulnerable to earthquakes, landslides and volcanic eruptions. These disasters are to some extent able to generate tsunamis (see again, the detailed discussions on Chapter Two). As a result, the government has the obligation to prevent the public from fatalities by taking action to reduce risks and running well-designed contingency plans to minimise the impact.

Figure 6.9. Both the authorities and related agencies work together on socializing disaster risk for local community at risk and doing action in best practices for evacuation in village and school

(taken from the 9th International Graduate Students and Scholars Conference in Indonesia by Surono, Yogyakarta on 9-10 August 2017).

Figure 6.9 shows good collaboration between the authorities and disaster agencies to socialise disaster issues through group gathering and educational approaches. Currently, a law on disaster management has been available for public: Law Number 24 of 2007. This law provides a basic guideline that regulates the rights, obligations and sanctions for all parties that are relevant to disaster management program. According to this law, the implementation of disaster management and associated action includes: (a) disaster prevention and preparedness, performed before an event; (b) timeless early warning, people evacuation and life protection, performed before and during an event; and (c) site reconstruction and rehabilitation, and people relocation, performed after an event.

As part of mitigation strategies, collaborative activities organised by the regional and central authorities as well as relevant agencies include socialising tsunami potential and its consequences in varying regions vulnerable to tsunami waves, in which estimates of tsunami height, tsunami inundation and tsunami arrival time are delivered to public under supervision by BMKG, BNPB and BPBD (see Fig. 6.10).

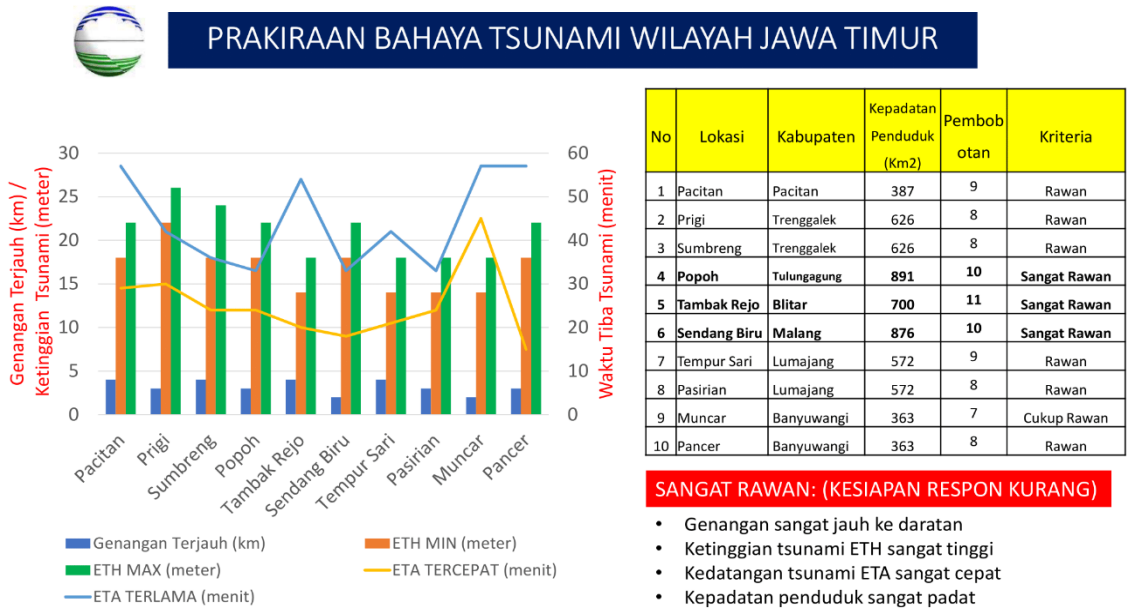

No	Lokasi	Kabupaten	Kepadatan Penduduk (Km2)	Pembobotan	Kriteria
1	Pacitan	Pacitan	387	9	Rawan
2	Prigi	Trenggalek	626	8	Rawan
3	Sumbreng	Trenggalek	626	8	Rawan
4	**Popoh**	**Tulungagung**	**891**	**10**	**Sangat Rawan**
5	**Tambak Rejo**	**Blitar**	**700**	**11**	**Sangat Rawan**
6	**Sendang Biru**	**Malang**	**876**	**10**	**Sangat Rawan**
7	Tempur Sari	Lumajang	572	9	Rawan
8	Pasirian	Lumajang	572	8	Rawan
9	Muncar	Banyuwangi	363	7	Cukup Rawan
10	Pancer	Banyuwangi	363	8	Rawan

Figure 6.10. Tsunami alert in East Java with estimated values of some tsunami parameters, such as tsunami height, inundation, arrival time, population densities and emergency status in regions of interest (taken from Peta Bahaya Tsunami Jawa Timur dan Kesiapan Respons by S. Pribadi and T. Yatimantoro, UPT Geofisika Jawa Timur, a webinar series of disaster mitigation study on 28 May 2021).

Disaster prevention and preparedness play an important role in building the resilience of communities. A well-structured plan for disaster prevention and preparedness is likely to be a written, approved, implemented, and periodically tested program, specifically outlining actions to be taken to reduce disaster risk and minimise the loss. The plan is therefore designed on the basis of a critical and thorough review of a possible disaster, such as a tsunami strike to specific geographic locations (see again, Fig. 6.10).

To sum up, tsunami disaster mitigation can thus be interpreted as all efforts and actions performed to prevent public from fatalities and to reduce tsunami impact to a minimum. Concerning with several possible causes of tsunami generation, including earthquakes of tectonic origin, landslides and volcanic eruptions (three types of geological disasters frequently occurred in the country) and the dense population living nearby coastlines, tsunami mitigation study focusing on necessary actions performed before, during and after a tsunami is of significance. The roles of the government and the relevant agencies at regional and national scales are therefore important.

6.4 Roles of Educational Institutions

Disaster risk reduction (DRR) education is the best thing to do by teachers and scholars to promote hazard assessment and risk analysis in either schools or universities through the implementation of disaster mitigation study to both school and university curricula. Efforts and discourses of the basic needs to integrate DRR into a science curriculum for university students in Indonesia are well documented. However, university lecturers and academics need more room to introduce the concepts of DRR education in a way that involves university students as experiential learners. Integrating DRR into Science, Technology, Engineering, and Mathematics (STEM) subjects is then a critical point, with which integration between subjects in STEM as well as other related subjects including the science of disasters and disaster management to apply in real life is plausible.

In the STEM-DRR approach, specific tools, such as hardware, software, applications associated information literacy practices are best used to guide students towards a better understanding of the subject matter, including tsunami disaster mitigation. In principle, this approach is all about how to use technology to deliver science concepts of disasters in a way that enhances student learning experiences. In this context, geoscience students are urged to be actively involved in understanding disasters under direct investigation through outdoor learning activities in order to develop deeper inquiry. Unfortunately, the outdoor learning environment is not yet commonly used as an integral component of

the geoscience learning process, where geoscience classrooms responsible for promoting tsunami mitigation strategies remain centred in textbooks readings and practical work undertook in the indoor environment. It is of main concern whether an alternative way of teaching disaster education and management that include tsunami disaster mitigation is available with no need to learn both in the outdoor settings.

In collaborative research facilitated by the university, Anggaryani et al. (2023) reported the use of virtual reality (VR) as an effective pedagogical tool for technology-enhanced learning through experience to promote STEM-DRR education. The study was aimed at determining the effects of the VR use on students' experiential learning about disasters, including tsunamis, where ten final-year student served as participants to use VR media. Significant contributions to the learning processes were observed during the process, where the majority of the participants argued in favour for the VR media, addressing successful completion of integrating STEM-DRR into the VR media content to promote students' awareness of tsunami risk.

6.5 Exercises

Answer clearly to the following questions regarding the content of Chapter Six.

1. How would you describe a tsunami to someone who had never seen one ?
2. What is the difference between tsunami hazard and tsunami risk regarding a potential tsunami disaster ? Does knowledge come into influence on the difference ? Why ?
3. Based on risk analysis, how do we assess the danger posed by tsunami vulnerability ?
4. Clearly explain in short argument, what kind of tsunami mitigation strategies relevant to low-lying coastal inhabitants with a lack of prior knowledge to a tsunami strike ?
5. What factors that may influence on the students’ perspectives and attitudes toward STEM-DRR education and tsunami risk analysis in Indonesia ?

This page is intentionally left blank

REFERENCES

1. Heidarzadeh M, Satake K, Takagawa T, Rabinovich A and Kusumoto S. 2018. A comparative study of far-field tsunami amplitudes and ocean-wide propagation properties: Insight from major trans-Pacific tsunamis of 2010–2015. *Geophysical Journal International*, Vol. 215, pp. 22-36.
2. Prastowo T, Bariyah AK, Cholifah L and Risanti H. 2022. Parameterising maximum tsunami amplitude with earthquake moment magnitude for trans-oceanic tsunamis. ASM *Science Journal*, Vol. 17.
3. Nishad P. 2021. *The Tsunami Handbook*. New Delhi, India: Vidya Books, pp. 1-174.
4. Farrell EJ, Ellis JT and Hickey KR. 2015. Chapter 4: *Tsunami Case Studies*. In Coastal and Marine Hazards, Risks and Disasters. Elsevier Inc. pp. 93-128.
5. Santellanes SR, Ruiz-Angulo A and Melgar D. 2022. Tsunami waveform stacking and complex tsunami forcings from the Hunga-Tonga eruption. *Pure and Applied Geophysics*, Vol. 180, pp. 1861-1875.
6. Hu G, Li L, Ren Z and Zhang K. 2023. The characteristics of the 2022 Tonga volcanic tsunami in the Pacific Ocean. *Natural Hazards and Earth System Sciences*, Vol. 23, Issue 2, pp. 675-691.
7. Muhari A, Heidarzadeh M, Susmoro H, Nugroho HD, Kriswati E, Supartoyo, Wijanarto AB, Imamura F and Arikawa T. 2019. The December 2018 Anak Krakatau volcano tsunami as inferred from post-tsunami field surveys and spectral analysis. *Pure and Applied Geophysics*, Vol. 176, No. 12, pp. 5219-5233.
8. Gusman AR, Supendi P, Nugraha AD, Power W, Latief H, Sunendar H, Widiyantoro S, Daryono, Wiyono SH, Hakim A, Muhari A, Wang X, Burbidge D, Palgunadi K, Hamling I and Daryono MR. 2019. Source model for tsunami inside Palu Bay following the 2018 Palu earthquake, Indonesia. *Geophysical Research Letters*, Vol. 46, No. 15, pp. 8721-8730.
9. Trujillo AP and Thurman HV. 2008. *Essential of Oceanography*. New Jersey, US: Pearson Prentice Hall, pp. 1-534.
10. Takabatake T, Han DC, Valdez JJ, Inagaki N, Mäll M, Esteban M and Shibayama T. 2022. Three-dimensional physical modeling of tsunamis generated by partially submerged landslides. *Journal of Geophysical Research*: *Oceans*, Vol. 127, Issue 1.
11. Fahmi MN, Realita A, Risanti H, Prastowo T and Madlazim. 2022. Back-projection results for the M_w 7.5, 28 September 2018 Palu earthquake-tsunami. *Journal of Physics*: *Conference Series*, Vol. 2377, 012032.

12. Heidarzadeh M and Mulia IE. 2022. A new dual earthquake and submarine landslide source model for the 28 September 2018 Palu (Sulawesi), Indonesia tsunami. *Coastal Engineering Journal*, pp. 97-109.

13. Grilli ST, Tappin DR, Carey S, Watt SFL, Ward SN, Grilli AR, Engwell SL, Zhang C, Kirby JT, Schambach L and Muin M. 2019. Modelling of the tsunami from the December 22, 2018 lateral collapse of Anak Krakatau volcano in the Sunda Straits, Indonesia. *Scientific Reports*, Vol. 9, No. 11946.

14. Giachetti T, Paris R, Kelfoun K and Ontowirjo B. 2012. Tsunami hazard related to a flank collapse of Anak Krakatau volcano, Sunda Strait, Indonesia. *Geological Society of London*: *Special Publication*, Vol. 361, pp. 79-90.

15. Paris R. 2015. Source mechanisms of volcanic tsunamis. *Philosophical Transactions of the Royal Society A*: *Mathematical*, *Physical and Engineering Sciences*, Vol. 373, Issue 2053.

16. Paris R, Switzer AD, Belousova M, Belousov A, Ontowirjo B, Whelley PL and Ulvrová M. 2014. Volcanic tsunami: a review of source mechanisms, past events and hazards in Southeast Asia Indonesia, Philippines, Papua New Guinea. *Natural Hazards*, Vol. 70, pp. 447-470.

17. Lynett P, McCann M, Zho Z, Renteria W, Borrero J, Greer D, Fa'anunu O, Bosserelle C, Jaffe B, Selle SL, Ritchle A, Snyder A, Nasr B, Bott J, Graehl N, Synolakis C, Ebrahimi B and Cinar GE. 2022. Diverse tsunamigenesis triggered by the Hunga Tonga-Hunga Ha'apai eruption. *Nature*, Vol. 609, Issue 7928, pp. 728-743.

18. Anderson JD Jr. 2009. *Chapter 2*, *Computational Fluid Dynamics*, 3rd ed JF Wendt (ed.) Berlin, Germany: Springer-Verlag, pp. 15-51.

19. Sorensen RM. 2006. *Chapter 2, Basic Coastal Engineering*, 3rd ed. New York, US: Springer, pp. 9-52.

20. Glimsdal S, Pedersen GK, Harbitz CB and Løvholts F. 2013. Dispersion of tsunamis: does it really matter? *Natural Hazards and Earth System Sciences*, Vol. 13, Issue 6, pp. 1507-1526.

21. Inazu D and Saito T. 2013. Simulation of distant tsunami propagation with a radial loading deformation effect. *Earth*, *Planets Space*, 65, 835-842.

22. Tsai VC, Ampuero JP, Kanamori H and Stevenson DJ. 2013. Estimating the effect of earth elasticity and variable water density on tsunami speeds. *Geophysical Research Letters*, 40, 492-496.

23. Wessel P. 2009. Analysis of observed and predicted tsunami travel times for the Pacific and Indian oceans. *Pure and Applied Geophysics*, 166, 301-324.

24. Watada S, Kusumoto S and Satake K. 2014. Travel time delay and initial phase reversal of distant tsunamis coupled with the self-gravitating elastic earth. *Journal of Geophysical Research*, 119, 4287-4310.

25. Hu G, Li L, Ren Z and Zhang K. 2023. The characteristics of the 2022 Tonga volcanic tsunami in the Pacific Ocean. *Natural Hazards and Earth System Sciences*, Vol. 23, Issue 2, pp. 675-691.

26. Realita A, Fahmi MN, Prastowo T, Tika NMASM and Madlazim. 2024. A Study on the 2022 Hunga Tonga-Hunga Ha'apai (HTHH) tsunami propagation: volcanic or meteo-tsunami ? *Journal of Physics*: *Conference Series*. Accepted for publication.

27. Aránguiz R. 2014. *Analysis of Tsunami Propagation in Coastal Areas*: *Lessons from Past Tsunamis*. Tokyo, Japan: Graduate School of Creative Science and Engineering, Waseda University, pp. 1-96.

28. Gelfenbaum G, Jaffe B, Watt S, Apotsos A, Richmond B, Buckley M and Peck B. 2009. *The Samoa Tsunami of September 29, 2009*: *Preliminary Field Data on Tsunami Inundation in American Samoa*. USDA Natural Resources Conservation Service, American Samoa Community College.

29. SATREPS Chile Tsunami Project. 2016. *Tsunami Basics for Engineering*. *Publication Series* Vol. 3. 1-46.

30. Esteban M, Takagi H and Shibayama T. 2015. *Handbook of Coastal Disaster and Mitigation for Engineers and Planners*. Oxford, UK: Butterworth Heinemann, pp. 1-765.

31. Anggaryani M, Prastowo T, Suprapto N, Lassa J, Madlazim, Alifteria FA, Agusty AI and Lestari NA. 2023. Virtual reality as experiential learning to promote STEM-DRR in tertiary education. ASM *Science Journal*, Vol. 18.

PENERBIT
PONPES JAGAD 'ALIMUSSIRRY (Anggota IKAPI)
" Komunitas Ilmuwan Spiritualis"